Environmental Pollution 403 (2026) 128400

Contents lists available at ScienceDirect

Environmental Pollution

journal homepage: www.elsevier.com/locate/envpol

Gaseous mercury fluxes from soils and health risk assessment at a coastal legacy industrial site

Federico Floreani [a,*], Antonella Vecchio [b,1], Maurizio Guerra [b], Elisa Mariani [b], Gianfranco Mulas [c], Stefano Covelli [a], Luca Spinelli [d], Giorgio Virgili [d,2]

[a] Department of Mathematics, Informatics and Geosciences, University of Trieste, Via E. Weiss 2, 34128, Trieste, Italy
[b] Italian Institute for Environmental Protection and Research (ISPRA), Department for the Geological Survey of Italy, Via V. Brancati 48, 00144, Rome, Italy
[c] Municipality of Portoscuso, Piazza Municipio 1, Portoscuso, SU, 09010, Italy
[d] Thearen s.r.l., Via E. De Sonnaz 19, 10121, Turin, Italy

ARTICLE INFO

Keywords:
Gaseous mercury volatilisation
Diffuse emissions
Contamination
Accumulation chamber
Inhalation risk assessment

ABSTRACT

A reliable estimation of gaseous elemental mercury (GEM) re-emissions from soils at mercury (Hg)-contaminated sites represents a key aspect for a proper health risk assessment for the local population, which may be potentially exposed through inhalation. This study investigates GEM fluxes at the soil-air interface within an area impacted by past local industrial emissions of Hg (Portoscuso, Italy) through a non-steady-state flux chamber (accumulation chamber) coupled to a real-time GEM analyser. Several flux measurements (n = 163) distributed over 5 selected sub-areas were performed, providing good spatial representativeness. Calculated GEM emission rates were used to assess indoor and outdoor human exposure according to the specific use of each area (e.g. residential or agricultural) by comparing them with values corresponding to acceptable exposure. Substantial GEM emissions (3.54–3164 ng m^{-2} h^{-1}) were observed for nearly all sampling points, with notable spatial heterogeneity partially related to meteorological factors and highest values mostly near the industrial complex. Comparable median fluxes were observed for urban settlements and arable areas (110 and 101 ng m^{-2} h^{-1}, respectively), highlighting the impact of land-use on GEM volatilisation. Overall, GEM emissions were below the estimated acceptable GEM flux for the site (Hazard Index<1), with the exception of 8 points randomly distributed over the study area and not likely indicative of a real unacceptable risk related to legacy re-emissions from contaminated soils. These results indicate that the adopted approach can be useful for large-scale preliminary investigations of GEM fluxes in Hg-contaminated sites, allowing point anomalies to be detected through direct field measurements.

1. Introduction

The occurrence of mercury (Hg) in the environment poses a serious threat to wildlife and human health due to the mobility, toxicity and bioaccumulation potential of its various chemical forms.

Although it is naturally present in all environmental media, since the industrial era several anthropogenic activities have greatly contributed to the increase of the amounts of Hg involved in natural exchanges between the atmosphere and terrestrial and aquatic ecosystems (Enrico et al., 2017; Selin, 2009). These activities include Hg mining and its use for the extraction of precious metals through amalgamation, fossil fuel combustion, the chlor-alkali industry, metal smelting, polymers and cement production, waste incineration (UNEP, 2019). It is estimated that more than 2/3 of historical Hg anthropogenic emissions affected local soils and waterbodies through direct discharges or fast atmospheric deposition of oxidised Hg (Hg^{2+}), whereas the remaining part was released into the atmosphere (Streets et al., 2019).

Once deposited on land or waterbodies, Hg can be re-emitted back into the atmosphere in its elemental form (Hg^0 or GEM, Gaseous Elemental Mercury). Thanks to its high volatility, GEM represents the main form of Hg in the atmosphere (>95% of the total; Mao et al., 2016) and can persist in this compartment for 0.8–1.7 years before being

* Corresponding author.
E-mail address: federico.floreani@units.it (F. Floreani).
[1] Current address: Italian National Institute of Health (ISS), Viale Regina Elena 299, 00161 Rome, Italy.
[2] Current address: Independent researcher.

https://doi.org/10.1016/j.envpol.2026.128400
Received 11 March 2026; Received in revised form 5 May 2026; Accepted 19 May 2026
Available online 21 May 2026
0269-7491/© 2026 The Authors. Published by Elsevier Ltd. This is an open access article under the CC BY license (http://creativecommons.org/licenses/by/4.0/).

removed through wet and dry depositions, allowing for a long-range redistribution (Ariya et al., 2015). As a result, the impact of anthropogenic Hg emissions can be detected even in remote pristine ecosystems (Fitzgerald and Clarkson, 1991; Sun et al., 2022).

Usually, most of the Hg derived from atmospheric depositions is present in the soil as Hg^{2+} bound to functional groups of soil organic matter or to mineral surfaces. However, desorption from these soil surfaces can increase the availability of Hg^{2+} for both vertical transport and reduction to volatile Hg^0 through biotic or abiotic pathways, resulting in the re-emission of previously deposited Hg from soil surfaces (Beckers and Rinklebe, 2017; Pannu et al., 2014). Several factors control these processes and subsequently GEM volatilisation. These include Hg content in the substrate, incident solar radiation, soil and air temperature, soil moisture, abundance and composition of organic matter, presence of vegetation and litter, soil disturbance, and the composition of the microbial community (Carpi et al., 2014; Fritsche et al., 2008; Kocman and Horvat, 2010; Kondo et al., 2024; Nacht et al., 2004).

As a legacy of past anthropogenic activities, soils around former facilities where Hg was produced and/or used (e.g. abandoned mines or chemical production facilities) usually show notably high contents of this metal (Bavec et al., 2015; Eckley et al., 2015; Grangeon et al., 2012; Osterwalder et al., 2019). At these contaminated sites, the primary focus is often the estimation of Hg transport to waterbodies and of the potential methylation and bioaccumulation in downstream environments (Eckley et al., 2020). However, due to the high Hg content, soils at these contaminated sites can emit considerable amounts of GEM to the atmosphere long after the contamination source has been phased out, potentially resulting in high atmospheric GEM concentrations (Fantozzi et al., 2013; Floreani et al., 2023a; Zhu et al., 2018). Consequently, the quantification of GEM re-emissions from soil surfaces is crucial for a proper health risk assessment for the local population. However, reliable quantifications of GEM emitted from these sites remain scarce, mostly due to the lack of a standard measurement protocol (Kocman et al., 2013; Osterwalder et al., 2019).

Field techniques for GEM emission estimation include flux chambers or micrometeorological approaches (relaxed eddy accumulation, modified Bowen ratio or aerodynamic gradient). The latter cause a marginal disturbance of the environmental conditions and can provide flux measurements on an ecosystem-scale, but require complex instrumentation to achieve fast and synchronous responses in measuring the various parameters, high computing capacity and personnel expertise. Conversely, flux chambers are relatively low-cost, versatile, portable and easy to handle, but are characterised by a reduced footprint and can alter the microclimatic conditions during measurements. The most widely used technique for measuring soil-air GEM fluxes is represented by dynamic steady-state flux chambers (DFC), where emissions are calculated from the gas flow rate and the difference between the concentrations in air entering and leaving the chamber (Eckley et al., 2010; Sommar et al., 2020; Zhu et al., 2016). However, with this approach, relatively long times are usually required to achieve a steady-state of the GEM concentrations inside the chamber, thus increasing the change in environmental conditions at the point of measurement. An alternative to the direct measurement of gas fluxes from soils is represented by non-steady state (NSS) flux chambers (or "accumulation chamber"), further categorised as flow-through or non-flow-through according to the presence or absence of continuous air recirculation within them (Livingston and Hutchinson, 1995; SNPA, 2018). In this case, flux calculation is based on the gaseous analyte concentration increase inside the chamber during the time of monitoring (Heinemeyer and McNamara, 2011). Compared to DFCs, NSS chambers are less sensitive to pressure differences induced by gas flow and are usually characterised by simpler designs. Pressure gradients are often minimised through vent openings; however, poorly designed vents could cause the disruption of internal fluid dynamics due to the Venturi effect at the opening, mostly in windy conditions, altering the diffusive flux from soils (Bain et al., 2005; During et al., 2009). Moreover, NSS chambers could be affected by perturbations induced by the extraction of the sample air volume and by gas recirculation, which could create a differential pressure and result in incomplete mixing of the vapours inside the chamber (Conen and Smith, 1998; Xu et al., 2006).

If coupled with real-time online analysers, NSS chambers require very short accumulation times, mostly in the case of high fluxes, minimising the impact on local microclimatic conditions (e.g. temperature and humidity) induced by any flux chamber method (Oertel et al., 2016; Pumpanen et al., 2004). The rapidity of flux measurements with NSS chambers allows for high spatial coverage and, subsequently, an estimation of diffuse gas releases from relatively large areas. Therefore, this approach could be useful for screening purposes at contaminated sites, with the aim of identifying high-emission areas. Despite this, NSS chambers have only rarely been employed for GEM flux measurement at contaminated sites (Di Francesco et al., 1998; Floreani et al., 2023a), whereas a more extensive application is reported for monitoring GEM degassing at volcanic areas (Cabassi et al., 2021; Sun et al., 2025, 2020; Tassi et al., 2016). The aim of this work was to test the application of an NSS continuous flow-through chamber to assess GEM fluxes at the soil-air interface within legacy industrially contaminated areas around the town of Portoscuso (SW Sardinia, Italy). The objective of the present study was not primarily centred on a mechanistic investigation of the environmental drivers regulating GEM emission kinetics. Rather, it maintains a strong operational focus, aimed at assessing site-specific risk through a Tier 2/Tier 3 approach. Specifically, this work provides a targeted investigation of areas previously identified as potentially critical during Tier 1 preliminary risk assessment, refining exposure scenarios through the direct measurement of soil-to-air GEM fluxes.

Results were used to assess the potential health risk for local inhabitants specifically related to GEM re-emissions from contaminated soils under different exposure scenarios. Within the framework of contaminated site management, health risk assessment is commonly conducted through a stepwise, risk-based approach (e.g. ASTM-RBCA), where increasingly site-specific data are progressively introduced to reduce uncertainty and support decision-making. In this context, the present study aims to provide a conservative evaluation by integrating direct measurements of GEM fluxes into standard exposure models. As a precautionary approach, measurements were conducted under the worst-case conditions most favourable to observe high GEM fluxes at the soil-air interface, namely high radiation and temperature (Kocman and Horvat, 2010). The performed risk assessment, in accordance with regulatory guidelines, aims to identify localised anomalies in emissions from soils that can cause potential harm to the exposed population. As such, the results are primarily meant to support risk management on a long-term rather than provide a comprehensive characterisation of actual human exposure. Potential impacts were evaluated considering the local population distribution and prevailing land-use settings, through the definition of representative exposure scenarios. This approach allows for a consistent assessment of reasonable maximum inhalation exposure for the different receptors potentially present within the study area.

Finally, the development of relatively simple and innovative protocols for monitoring and assessing the fate of Hg in contaminated sites is crucial for the implementation of the Minamata Convention (Selin et al., 2018). From this point of view, the information gathered in this study may also be useful for assessing the feasibility of the proposed approach as a simple tool to support risk assessment and the choice of management strategy for Hg-contaminated sites.

2. Materials and methods

2.1. Study area

Field measurements were conducted in five selected “macro-areas” in the surroundings of the town of Portoscuso, South-Western Sardinia, Italy (Fig. 1). The area lies on a coastal plain consisting of Quaternary

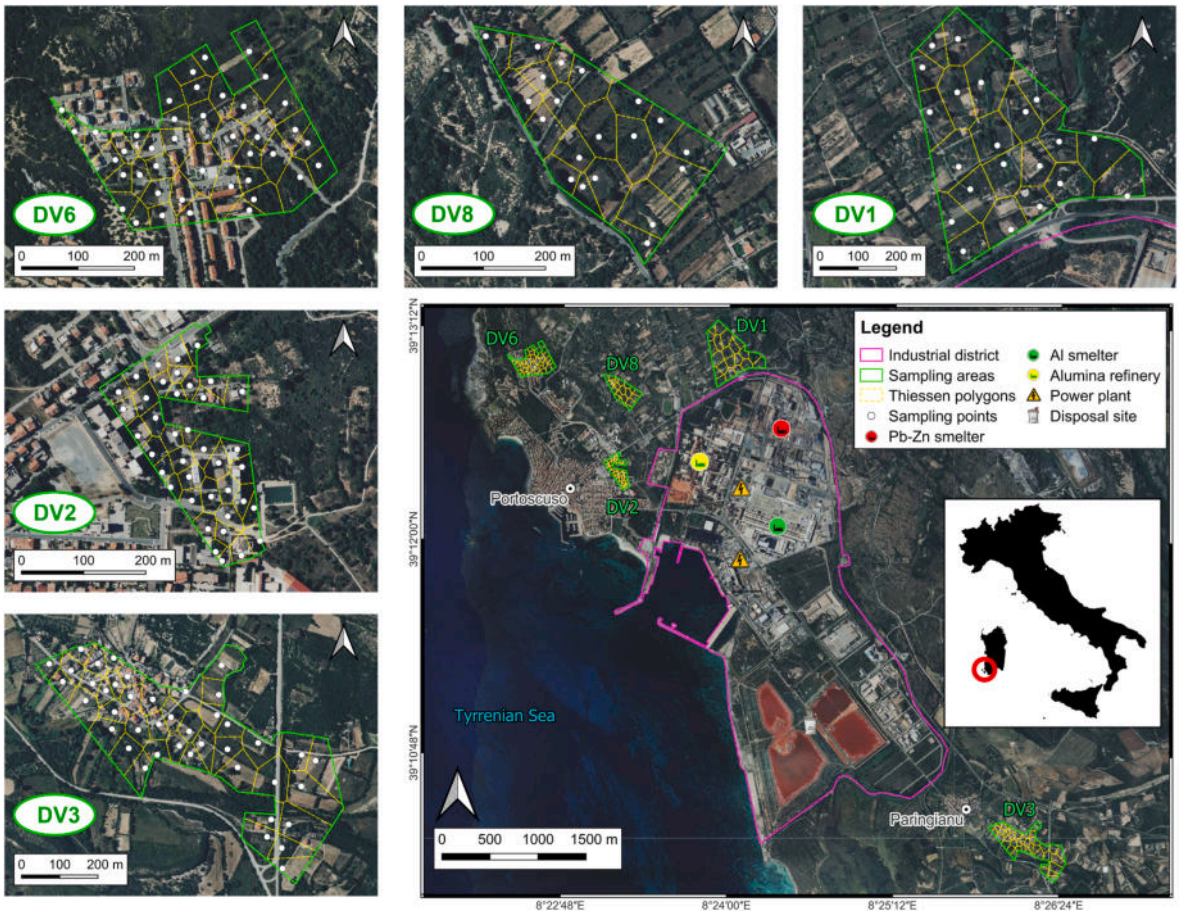

Fig. 1. Index map of the study area (in the right bottom corner) and distribution of sampling points within the selected sampling macro-areas.

deposits, with a thickness ranging from 80 to 100 m along the shoreline to a few metres or less in the inland sector, composed of yellowish-reddish, moderately compacted silty and sandy-silty deposits. This unit overlies an impermeable marly-clayey layer, Paleogene volcanic rocks (trachytes and ignimbrites), and a layer composed of tuffites and conglomeratic continental deposits characterised by an ash-pumice matrix (Cixerri Formation). According to the World Reference Base for Soil Resources (WRB), dominant soil types are Mollic Andosols and, to the south-east, Eutric Cambisols, with a prevalent loam or sandy-loam texture (Aru et al., 1991; FAO and IIASA, 2008). A 5–30 cm thick surface aeolian sandy layer resulting from erosion and transport of coastal deposits covers the entire area (APAT, 2008).

The isobioclimate of the area is Mediterranean Pluviseasonal-Oceanic with lower dry to upper dry ombrotype (Canu et al., 2015). Mean annual precipitation ranges between 486.5 and 548.1 mm (data 1981–2010; ARPAS, 2020), with winter peaks and a dry period during summer. Mean monthly temperatures range between 10.3 °C in February and 26.7 °C in July.

Natural vegetation biome consists of Mediterranean shrub, including Sardinian psammophilous geosigmetum of coastal dunes and thermo-Mediterranean series of wild olive (*Asparago albi-Oleetum sylvestris*), replaced inland by the Sardinian calcifuge series of cork oak (*Galio scabri-Quercetum suberis*) (Bacchetta et al., 2009). Anthropogenic activities have heavily modified the natural environment within the study area. Soils are frequently devoted to arable (mainly cereals and fodder) or perennial crops (vineyards or olive groves), whereas grasslands in low-lying areas are often used for grazing. The two main urban areas are the town of Portoscuso, and the small village of Paringianu, located in the southern part of the study area. These urban, agricultural, and semi-natural land-use settings are associated with different population presence and activity patterns, which were explicitly considered in the definition of exposure scenarios adopted in the risk assessment.

The main anthropogenic pressure is the Portovesme industrial district (Fig. 1), which includes a lead-zinc smelter, coal- and oil-fired power plants, an aluminium smelter, and an alumina refinery with a large disposal site for red muds (Schintu et al., 2005; Vecchio et al., 2012). Since 1975, the smelter has produced also Hg from sphalerite, with an annual production about 9–17 t (Schintu et al., 2005; Schintu and Degetto, 1999). Atmospheric emissions and subsequent depositions related to these industrial activities are considered the primary source of soil contamination in the surrounding areas, resulting in the widespread occurrence of various potentially toxic elements (e.g. As, Cd, Hg, Pb, Sn, Zn) (Vecchio et al., 2015). Consequently, the area of the municipality of Portoscuso is included in the Contaminated Site of National Interest (SIN) "Sulcis-Iglesiente-Guspinese" following Italian Ministerial Decrees 468/2001 and 304/2016.

2.2. Soil-air GEM flux measurements

The selection of sampling sites was conducted according to a targeted, risk-based approach, integrated with the findings of a recently performed, preliminary site-specific human health risk assessment. Five representative macro-areas (DV1, DV2, DV3, DV6, and DV8; Fig. 1) were defined by clustering several "critical polygons" (Fig. S1c). These polygons were previously identified as hotspots where top-soil total Hg concentrations exceeded the Risk Threshold Concentrations for specific exposure pathways, namely direct soil contact and, crucially, indoor and outdoor inhalation of vapours. Accordingly, the present study was not aimed at an independent reassessment of the entire site, but to a targeted, site-specific refinement of previously identified risk scenario with

a risk based stepwise framework. Such an iterative approach is commonly adopted in the management of contaminated sites to reduce uncertainty and support operational decision-making. Two of the macro-areas (DV2 and DV6) comprise mainly urban environments, while the other two (DV1 and DV8) are prevalently used for agriculture or grazing. The fifth macro-area (DV3) includes both environmental settings and is located south-east of the industrial area.

Measurements to assess GEM fluxes at the soil-air interface were conducted at the beginning of June 2021 for five consecutive days, one for each of the macro-areas selected above. Measurements were performed during daytime, approximately between 08:30 and 18:30 local time.

Within each macro-area, sampling points were placed as close as possible to the centroid of Thiessen polygons delineated to represent the areas identified as critical following the soil risk assessment for Hg contamination. Soil cover (e.g. urban soils, farmland, shrubland, etc.) was also taken into account when selecting sampling locations to measure fluxes in environmental conditions more representative of those prevailing for the soils of each polygon.

GEM fluxes were measured using a cylindrical (Ø = 40 cm, h = 10 cm) NSS flux chamber ("accumulation chamber", Fig. S2) made of Plexiglas (polymethylmethacrylate). This material was chosen due to its durability and good transmission (80-90%) of visible and UV-A radiation (315-400 nm), essential to obtain a reliable estimation of GEM fluxes (Carpi et al., 2007; Wang et al., 2006), whereas UV-B radiation (280-315 nm) is partially filtered. Although this radiation is the most effective in promoting Hg photoreduction (Moore and Carpi, 2005), it represents only a small portion of total radiation reaching the soil. The flux chamber used in this study is similar to experimental designs found in the literature and frequently used for the determination of greenhouse gases and VOC emissions (e.g. Cardellini et al., 2003; Chiodini et al., 1998; Gallego et al., 2014; Schroder et al., 2016).

The chamber was coupled with a real-time portable GEM analyser (Lumex RA915M; Lumex Instruments, St. Petersburg, Russia). This instrument allows for the determination of GEM concentrations over a wide dynamic range (2–30,000 ng m^{-3}) through differential atomic absorption spectrometry with Zeeman background correction (Sholupov et al., 2004). Calibration is performed annually by the parent company and accuracy was checked in the field before starting measurements thanks to an internal reference cell containing a known amount of Hg. The obtained results were $\leq$ 5%, complying with the quality criterion indicated in the instrument manual ($\leq$ 20%).

Flux measurements were taken by placing the chamber directly on the soil surface with the edges inserted 1-2 cm into the soil. Surface vegetation and litter, if present, were carefully removed before measurements and surface roughness was gently flattened. A thin layer of soil was gently applied to the outer rims of the chamber to achieve optimal sealing and prevent the intrusion of external air, which could cause biases in flux estimation (Gillis and Miller, 2000). Two tubes attached to holes in the upper wall of the chamber provided the connection to the GEM analyser. The air was continuously recycled inside the chamber by means of the internal pump of the Lumex analyser at a constant rate of at least 10 L min^{-1}. During deployment, GEM concentrations in the recycled air were continuously measured with a sampling interval of 1 s and displayed on the digital display of the Lumex. This allows for a preliminary in-field evaluation of the GEM emission rate from the surface based on the observed increase of concentrations in the headspace air. Inlet and outlet holes have a small curved portion of tubing inserted inside the chamber in order to obtain a homogeneous air flow and a proper mixing of the inside air (Pumpanen et al., 2004). A ventilation opening with a porous septum on the upper wall was used to minimise the inflow of outside air while still allowing pressure to be balanced (Hutchinson and Livingston, 2001). The monitoring duration at each point was set to 5 min, an interval commonly adopted for measurements with accumulation chambers coupled with real-time online analysers (Maier et al., 2022) and sufficient to observe a linear increase in GEM concentrations in the air in the chamber headspace. GEM fluxes (F, in ng m^{-2} h^{-1}) were calculated based on the increase in GEM concentrations over time (dC/dt) according to Equation (1):

$$F = \frac{dC}{dt} \cdot \frac{V_c}{A_c} \cdot \frac{3600 \cdot P_a \cdot 100}{10^6 \cdot R \cdot (T_a + 273.15)} \quad (1)$$

where V_c is the chamber internal volume (0.01256 m^3), A_c is the basal area of the chamber (0.1256 m^2), P_a is the atmospheric pressure (in Pa), T_a is the air temperature (in K) and R is the gas constant (8.314 m^3 Pa K^{-1} mol^{-1}). The increase in GEM concentrations was quantified as the slope of the GEM vs. time in the portion characterised by a good linear trend ($R^2 > 0.80$) over an at least 180-sec interval (Chiodini et al., 1998; Kyllönen et al., 2012). The regression was performed on the first representative portion of the curve, when the internal conditions are still comparable to the external environment. Automatic calculation algorithms were applied to minimise analyst subjectivity in the selection of the curve integration intervals. Chamber blanks were performed on a clean plastic surface before and after each sampling period and the mean value (2.07 ± 2.28 ng m^{-2} h^{-1}, n = 10) was subtracted to the calculated flux.

At the same time, a second smaller sampling line was connected to an infrared CO_2 analyser (LI-820; LI-COR Environmental, Lincoln, USA) to measure CO_2 fluxes at the soil-air interface with the same approach described above. This analyser aspires air at a lower flow rate (1 L min^{-1}) and allows for the determination of air CO_2 concentrations in the range 0.1-20,000 ppm with an accuracy of < 3%. Similar to GEM, CO_2 concentrations were recorded continuously during measurements. In this case, the variation of CO_2 concentrations in the chamber headspace was displayed in real-time on a graph shown on a laptop. Since CO_2 efflux related to soil respiration always occurs in soils as a part of the terrestrial carbon cycle (Kuzyakov, 2006; Raich and Schlesinger, 1992), this measurement was used to verify the functioning of the sampling equipment: deviations from the linear increase of CO_2 concentrations were considered indicative of an intrusion of external air due to a non-perfect chamber sealing with the soil. The real-time visualisation of these data allowed for the immediate identification of invalid measurements, which were then repeated in the field.

Atmospheric temperature and pressure were monitored in the field through portable probes. Moreover, incident UV radiation between 250 and 400 nm was continuously monitored during the entire sampling period through a specific sensor (SU-420; Apogee Instruments, Logan, USA) mounted at ~2 m height in a fixed location within the sampling macro-areas.

Statistical analysis of GEM fluxes and ancillary measured parameters were performed through R software ver. 4.5.2 (R Core Team, 2025). Data normality was checked through Shapiro-Wilk test. As GEM flux data showed a non-normal and highly skewed distribution, non-parametric Kruskal-Wallis coupled with Dunn's post-hoc tests were used to assess differences among fluxes observed in the various macro-areas or land use categories. For the same reason, Kendall correlation coefficients were used to make a preliminary assessment of the relationships among the variables. Conversely, log-transformed data were used for multiple linear regression analysis coupled with dominance analysis to evaluate the relative independent contributions of each factor on GEM fluxes. *Dominanceanalysis* (Bustos Navarrete and Coutinho Soares, 2025) and *ggplot2* (Wickham, 2016) R packages were used for dominance analysis and data visualisation respectively.

2.3. Risk assessment

The human health risk assessment was performed according to the Italian technical guidelines for vapour monitoring at contaminated sites (SNPA, 2018), which are based on international standard guidelines on evaluation and clean-up of contaminated sites (ASTM, 2001; US EPA,

1996). According to a risk-based stepwise approach, the adopted methodology represents an intermediate-to-advanced assessment level, where site-specific measurements are used to reduce the uncertainty associated with purely analytical emission models, while still relying on conservative modelling assumptions to ensure protection of human health. If the investigated area also includes buildings, these guidelines provide for the assessment of exposure in both outdoor and indoor environments.

Potential exposure to Hg through inhalation and its associated risk are evaluated through estimated GEM concentrations in the air, which were calculated from the soil-air GEM fluxes measured in the field with the flux chamber. Calculation of atmospheric GEM concentrations (C_{air}) is based on different mixing models assuming fully mixed outdoor/indoor environments. For the outdoor environment, the box model (Equation (2)) was applied:

$$C_{air-outdoor} = \frac{F \cdot L_{wind}}{v_{wind} \cdot \delta_{air}} \quad (2)$$

where F is the measured GEM flux, L_{wind} is the source length along the prevailing wind direction, v_{wind} is the mean wind speed (calculated from data recorded by the Portoscuso meteorological station) and δ_{air} is the height of the mixing layer (fixed at 2 m). Concentration of GEM in the air for the indoor environment was estimated taking into consideration the mixing in confined environments (Equation (3)) (Johnson and Ettinger, 1991):

$$C_{air-indoor} = \frac{F \cdot A_B}{V_B \cdot ER_B} \quad (3)$$

where A_B and V_B are respectively the exchange surface and volume of the building and ER_B is the air exchange rate. These parameters were estimated based on the types of buildings present in each area according to the municipal urban plan.

Four different exposure scenarios were considered: i) residential land use, ii) mixed residential-agricultural land use, iii) recreational, and iv) sporadic/pasture. The potentially exposed population was characterised through scenario-based representations reflecting land-use, building typology, and typical occupancy patterns of the investigated areas, as defined in the municipal urban plan. Sensitive receptors were considered following the standard regulatory practice and include children (0-6 yrs), teenagers (7-16 yrs), adults (17-65 yrs), and seniors (> 65 yrs), to account for differences in inhalation rates, exposure duration, and vulnerability. This population characterisation is consistent with the health-protective objectives of the adopted risk assessment framework. Acceptable GEM concentrations in the air (C_{acc}), defined as the maximum value corresponding to the acceptable health risk (Hazard Index = 1), were calculated for each scenario and sensitive receptor. The exposure parameters used for the estimation of the C_{acc} are listed in Table S1.

As a precautionary approach, the lowest C_{acc} obtained for the different age classes in each scenario was used to calculate the corresponding acceptable GEM flux (F_{acc}) at the soil-air interface. The values of F_{acc} in the various scenarios were obtained by solving Equations (2) and (3) for the estimated C_{acc} and were then compared with the specific GEM emission rates for each area and each polygon to evaluate the potential health risk through inhalation in the various scenarios.

The relative contribution of each polygon to the overall GEM emissions for each selected macro-area is represented by the product between the measured flux and the area of the corresponding polygon. Specific GEM emission rates were then obtained as the ratio between the sum of the relative contributions of each polygon and the total surface area of the investigated macro-area. All calculations were carried out using an Excel spreadsheet.

3. Results and discussion

3.1. Ancillary parameters

Overall, GEM fluxes were measured at 163 sampling points within the study area during the five days of field activity. Summary statistics of measured GEM and CO_2 fluxes at the soil-air interface together with the mean incident UV radiation and air temperature are reported in Table 1. Mean UV radiation was calculated considering the data recorded exactly in parallel with each single flux measurement.

Field measurements were performed in mostly sunny conditions except for those conducted at DV3 in the morning and at DV2. In these cases, light intermittent cloud cover was encountered, resulting in a slightly lower mean values with regard to UV radiation and in a more irregular diel pattern than in other areas (Fig. 2). Nevertheless, at DV3 the maximum value recorded in parallel with a single flux measurement (52.0 W m^{-2}) was found, thus indicating a notable UV radiation despite cloud cover. No rain occurred during the entire sampling period. The lowest values of UV radiation were usually recorded during the few measurements conducted in the early morning (approximately before 9:00) or late afternoon (after 17:30), with minimum values observed in the morning at DV2 (< 5 W m^{-2}).

Air temperature recorded during field activities ranged between 20.2 and 28.7 °C with no significant differences between the values measured on different days (Fig. 2). Generally, air temperature was constantly above 25 °C between 11:00 and 18:00 local time. Conversely, lower values were observed during the first measurements conducted in the morning, mostly at areas DV8 and DV2.

Carbon dioxide fluxes at the soil-air interface were measured simultaneously with GEM fluxes at each sampling point to monitor chamber sealing integrity to the soil through real-time visualisation of CO_2 headspace concentrations. Positive CO_2 fluxes were observed at almost all sampling points, with good linearity in the variation of headspace concentrations. This rules out significant leaks or the intrusion of external air which could have biased the determination of GEM fluxes. Overall, CO_2 fluxes ranged between 0.71 and 573 mg m^{-2} h^{-1} (Fig. S3), with the highest median value recorded for the DV2 macro-area and the lowest for DV3 (Table 1). No discernible spatial trends or clusters were observed in the distribution of CO_2 fluxes at the soil-air interface. This may be related to the high heterogeneity of environmental contexts in which the measurements were conducted, ranging from urban to farmland soils and natural unmanaged scrubland environments even within the same macro-area. This heterogeneity of environments and management practices can effectively lead to high variability in the various factors (i.e. soil temperature and moisture, organic carbon content, bulk density, microbial biomass composition) involved in CO_2 exchange with the atmosphere (Wagai et al., 1998; Weissert et al., 2016).

In the entire dataset only two negative values (−1093 mg m^{-2} h^{-1} at DV6-17 and −297 mg m^{-2} h^{-1} at DV8-7) were obtained, indicating a net sequestration of carbon in these soils. This could be related to abiotic processes (mineral weathering, CO_2 dissolution) coupled with low soil biotic respiration, as frequently observed in arid sandy soils (Dietzen and Rosing, 2023; Xie et al., 2009). However, even in these cases, good linearity was achieved in the decrease of internal CO_2 concentrations, confirming the excellent sealing of the chamber and the reliability of the corresponding GEM flux measurements.

3.2. GEM fluxes

Considering the complete dataset (n = 163) across the entire study area, GEM fluxes at the soil-air interface showed considerable variability, ranging between −104 and 3164 ng m^{-2} h^{-1} (points DV2-26 and DV6-28, respectively). However, most of the observed GEM fluxes (85% of the total) were below 200 ng m^{-2} h^{-1} (Fig. 3a).

GEM fluxes were extremely variable even within each single macro-

Table 1
Summary statistics of GEM and CO_2 fluxes at the soil-air interface, incident UV radiation, and air temperature measured in the five selected macro-areas.

		GEM flux (ng m^{-2} h^{-1})		CO_2 flux (mg m^{-2} h^{-1})	UV rad. (W m^{-2})	Air Temp (°C)
Area	N	Mean ± SD	Min – Max (Median)	Min – Max (Median)	Mean ± SD	Mean ± SD
DV1	21	172 ± 236	5.70 – 1032 (81.4)	37.7 – 445 (156)	33.9 ± 12.2	25.9 ± 1.6
DV2	39	192 ± 396	−104 – 2309 (87.4)	63.0 – 445 (195)	29.6 ± 15.9	25.1 ± 2.8
DV3	42	72.2 ± 92.1	3.54 – 441 (35.9)	0.71 – 347 (122)	26.1 ± 9.6	25.9 ± 0.9
DV6	41	160 ± 490	15.4 – 3164 (64.2)	−1093 – 476 (160)	34.4 ± 10.4	26.4 ± 1.6
DV8	20	90.8 ± 68.3	−44.0 – 195 (88.1)	−297 – 573 (137)	34.1 ± 8.0	25.9 ± 1.3

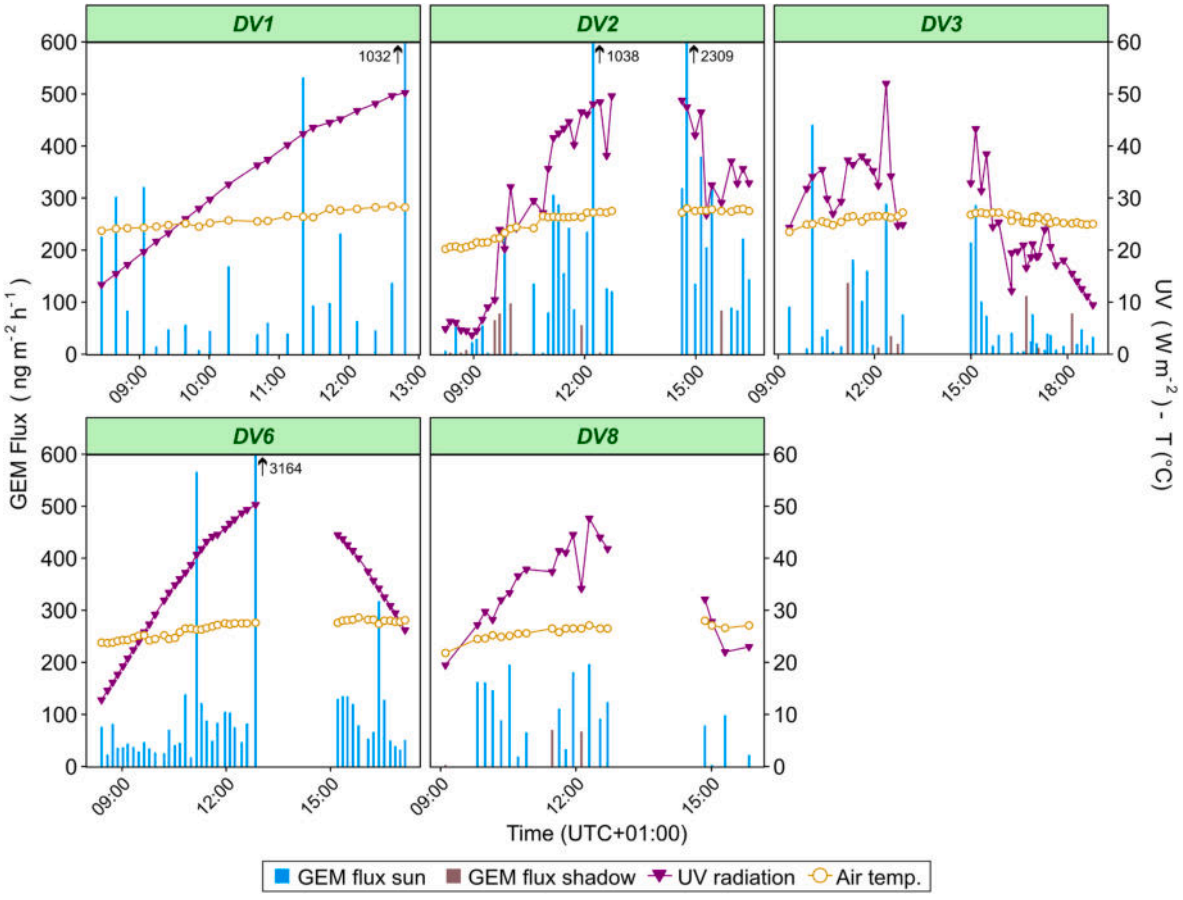

Fig. 2. Variation of GEM fluxes, UV radiation and air temperature during sampling periods in the five selected macro-areas.

area, as highlighted by the high values of standard deviations reported in Table 1. As regards CO_2 fluxes, this variability is related to the wide range of environments investigated in each macro-area. The complex site-specific interactions among the various influencing factors can indeed strongly affect the soil-air GEM exchanges (Liu et al., 2014; Rinklebe et al., 2010) and will be discussed later in the text.

Negative GEM fluxes were observed for only 7 points randomly distributed within DV8 and mostly DV2 macro-areas, whereas in only one point (DV2-14) it was not possible to obtain a good linear regression in the GEM concentration vs. time curve and therefore GEM flux could not be calculated (Kyllönen et al., 2012). For further elaborations, GEM flux at this point was set to 1.03 ng m^{-2} h^{-1} (1/2 of the chamber blank). Statistical analysis revealed no significant differences in GEM fluxes at the DV1, DV2, DV6 and DV8 macro-areas (Fig. 3a), with the highest emissions found at DV8 and DV2 (median = 88.1 and 87.4 ng m^{-2} h^{-1}, respectively). Conversely, slightly lower values were observed for DV3 macro-area, with a median GEM flux of 35.9 ng m^{-2} h^{-1}, significantly lower than those recorded at DV1, DV2, and DV8 ($p < 0.01$, $p < 0.05$ and $p < 0.05$ respectively, Dunn post-hoc test). These latter areas are those located closest to the industrial complex of Portovesme and thus were likely subject in the past to higher atmospheric Hg supplies due to anthropogenic releases, resulting in higher diffuse GEM re-emissions. This is further highlighted by the lower median values of GEM fluxes found at the DV6 and DV3 macro-areas (Table 1), located at increasing distances from the industrial complex. On the other hand, dispersion of GEM from the industrial area could still lead to the build-up of episodic high atmospheric levels even if Hg production and use have ceased, as observed elsewhere (Acquavita et al., 2017; Esbrí et al., 2018, 2020; Floreani et al., 2022). Depending on soil Hg concentration, elevated ambient GEM levels can suppress emission from the soil surface and lead to net deposition (Eckley et al., 2015). This could explain the negative fluxes observed only at some points in the DV2 and DV8 macro-areas. For example, brief 5-min measurements of GEM concentrations in the air taken at points DV2-26 and DV8-1, characterised by negative fluxes (−103 and −44.0 ng m^{-2} h^{-1}, respectively), showed notably high mean values (245 ± 4 and 149 ± 7 ng m^{-3}), supporting this hypothesis.

Overall, the GEM fluxes recorded in this study are clearly higher than those commonly observed in background areas not influenced by strong

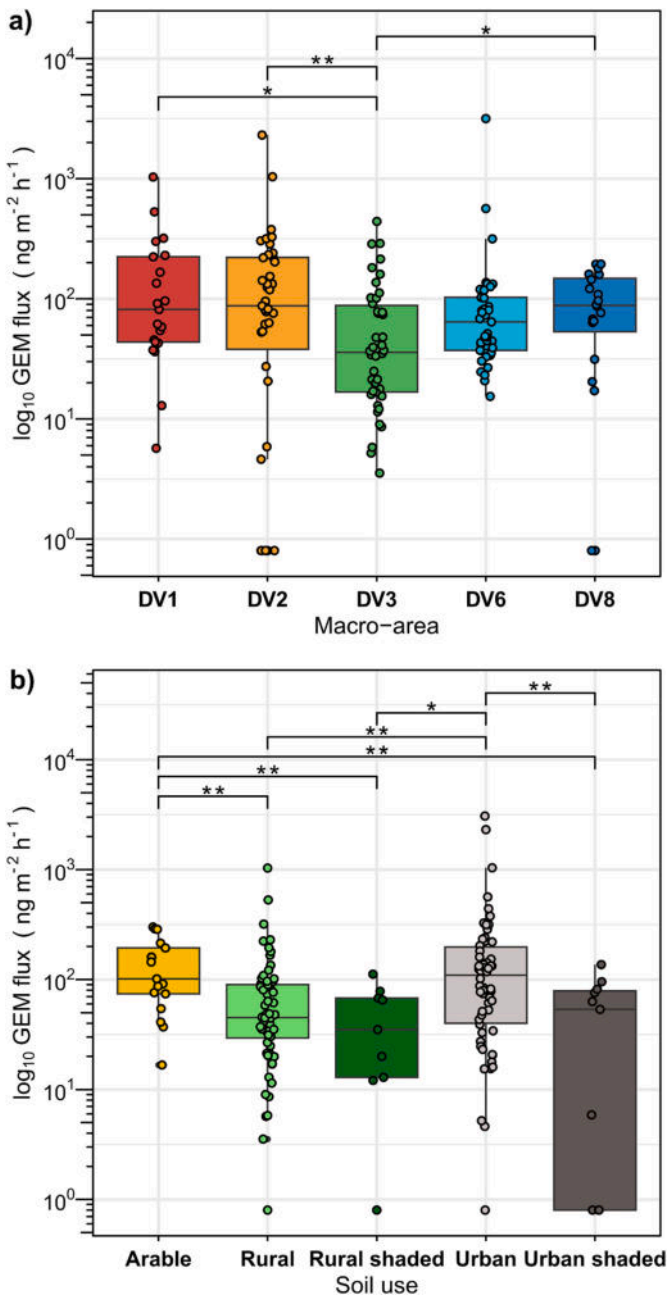

Fig. 3. Distribution of GEM fluxes at the soil-air interface in: a) the five investigated macro-areas; b) different soil use categories. Statistically significant differences according to Dunn post-hoc test are indicated by asterisks (* = $p < 0.05$; ** = $p < 0.01$).

anthropogenic inputs of Hg, which are estimated to be 1.2 ± 2.2 ng m^{-2} h^{-1} (mean ± SD) on a global level (Agnan et al., 2016). On the other hand, GEM fluxes in the same range as those found in this study are commonly observed at sites subject to Hg contamination due to past industrial activities. For example, GEM fluxes between 20 and 2114 ng m^{-2} h^{-1} were determined for the area around former chlor-alkali and polymers production facilities in Switzerland (Osterwalder et al., 2019), a metal smelter in Canada (up to 284 ng m^{-2} h^{-1}, Eckley et al., 2015) and a coal power plant in China (2–318 ng m^{-2} h^{-1}, Li et al., 2018). In these cases, the main contamination pathway is usually represented by atmospheric depositions, similarly to the soils from our study area (Schintu et al., 2005).

However, it must be stressed that the above-cited measurements were performed with the dynamic steady state flux chamber technique, the most widely used for monitoring GEM fluxes at the soil-air interface (Agnan et al., 2016; Sommar et al., 2020). Differences in chamber type (e.g. steady vs. non-steady state), shape, dimensions, material and air turnover rate may significantly influence the calculated flux value (Eckley et al., 2010). Therefore, comparisons between GEM fluxes reported in different studies using different measuring techniques should always be made with caution. GEM emissions significantly higher than those observed in this study has been widely reported for active volcanic and geothermal areas when measured with NSS chambers. Due to natural degassing, GEM fluxes observed in these areas with both static (Cabassi et al., 2021; Tassi et al., 2016) and flow-through chambers (Bagnato et al., 2014; Sun et al., 2020) can reach values up to thousands or tens of thousands of ng m^{-2} h^{-1}. In other areas impacted by human activities, an experimental approach similar to that adopted in this study was applied to evaluate GEM fluxes from soils to air at the Hg-mining impacted sites within the Isonzo River plain (Floreani et al., 2023b) and near modern and historic roasting sites at the Idrija mining district (Floreani et al., 2023a). Despite soil Hg concentrations being one to two orders of magnitude higher, GEM fluxes observed in these areas (37.6–1018.4 and 70.7–701.8 ng m^{-2} h^{-1}) were only slightly higher than those recorded at Portoscuso. This may be attributed to the different Hg forms present in these areas.

Mercury can occur in soils under various chemical forms characterised by different mobility and availability for reduction to Hg^0 and subsequent volatilisation (Schlüter, 2000). Generally, substrates where Hg occurs as cinnabar (α-HgS) are characterised by the lowest GEM emission rates due to the stability of this Hg form, which requires higher energy supplies to induce the release to the atmosphere compared to other Hg forms (Gustin et al., 2002; Llanos et al., 2011; Zhao et al., 2022). At sites subject to Hg supplies from atmospheric depositions such as the Portoscuso area, the prevalent Hg fraction is usually constituted by the so called "matrix-bound" Hg, potentially more available for reduction and subsequent volatilisation. Due to its high affinity for soil organic matter, mostly with sulphur-containing functional groups, Hg from atmospheric depositions is indeed easily adsorbed by soil organic matter retained in upper organic soil layers (Jiskra et al., 2015; Xia et al., 1999).

Unfortunately, only a few surface soil samples, with total Hg concentrations ranging between 320 and 2841 ng g^{-1} (Table S2), were available in this study to investigate the element speciation. These concentrations agree with those previously reported for topsoils collected for the first phase of risk analysis by local authorities (< 100 – 6900 ng g^{-1}; Fig. S1a). Relatively high values of total Hg were also reported for deeper soils (up to 1900 ng g^{-1}) (Fig. S1b). Available samples were used for Hg thermo-speciation analyses (Petranich et al., 2022) coupled with an oxidising treatment to assess the fraction of Hg bound to organic matter (Biester et al., 2000) according to the procedure described in detail in Text S1. The results of these determinations, although not fully representative of the whole area, are consistent with the above-described process. Given the absence of other known Hg sources, this result may nevertheless provide an indication of the prevalent form of this metal most likely to be found in soils of the study area. As can be seen in Fig. 4, in untreated samples, Hg was released at temperatures around 230 °C, but after the oxidation test this peak was strongly reduced or even disappeared. The amount of Hg lost through oxidation can be considered organically-bound Hg (Biester et al., 2000) and represented a significant portion (46.6–100%) of the total amount of this metal in the analysed soils (Table S2). This result may support the hypothesis of an atmospheric source of Hg in soils and consequently of the presence of Hg forms potentially more available for volatilisation relative to mining-impacted sites.

Although the present-day Hg inputs into the analysed soils have likely decreased due to more efficient emission control measures, the relatively high fluxes observed in our study confirm that GEM re-emissions can persist for several years before background conditions are restored, as is frequently observed at other historically contaminated

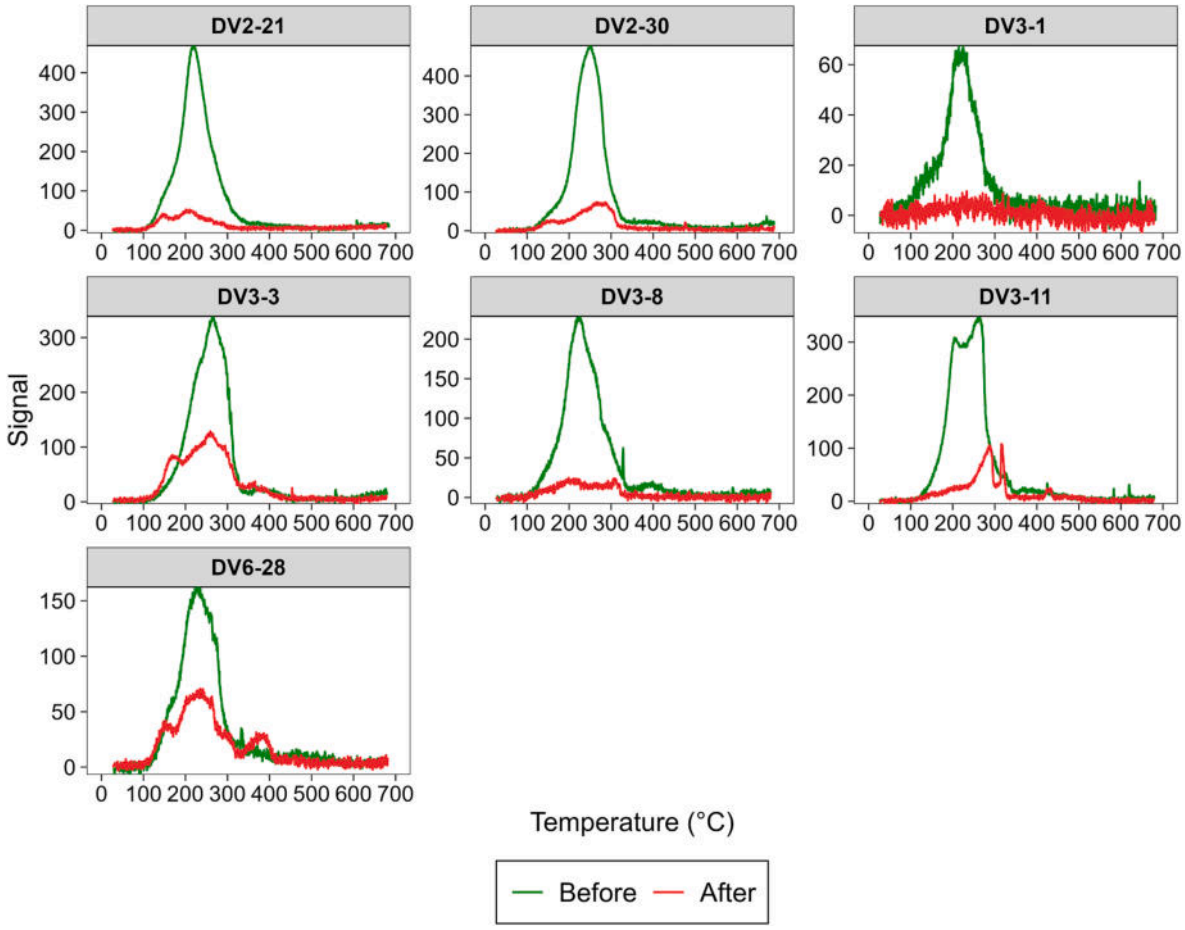

Fig. 4. Mercury thermo-desorption curves of selected soil samples before and after the oxidation test.

sites (Huremović et al., 2017; Zhu et al., 2018). Moreover, the decrease in atmospheric GEM concentrations due to the gradual elimination of industrial emission sources may lead to an increase in GEM re-emissions from contaminated soils, no longer limited by high atmospheric GEM levels. In extreme situations, removing a strong contamination source lowers atmospheric concentrations, thereby reversing the air-soil gradient and shifting GEM fluxes from deposition to net emission (Eckley et al., 2015).

The high spatial variability of GEM fluxes is also evident within each studied area, with extreme emission values often recorded in adjacent polygons (Fig. 5). As a result, no clear spatial trends were identified, indicating the absence of spatial autocorrelation. Therefore, the measured data precluded the application of geostatistical methods (Elío et al., 2016).

High small-scale spatial heterogeneity of GEM fluxes has frequently been observed from various substrates (e.g. contaminated soils, urban soils, mining residues) as a result of complex and site-specific interactions of several factors that can influence GEM volatilisation from soils, which is not only dependent on soil Hg concentration and speciation (Fu et al., 2012). These factors include both environmental conditions governing Hg reduction and translocation in soil, such as solar radiation, temperature, soil moisture, precipitation, and physical characteristics of soils like abundance and size of pores, vegetation type cover, surface compaction and anthropogenic disturbance (Eckley et al., 2011; Liu et al., 2014; Rinklebe et al., 2009). Among physical forcings, incident solar radiation has widely been recognised as one of the most relevant parameters in influencing the magnitude of GEM fluxes at the soil-air interface (Eckley et al., 2015; Kondo et al., 2024; Wang et al., 2005). Solar radiation, mostly in the UV wavelengths, favours the photoreduction of Hg^{2+} in surface soil layers (Moore and Carpi, 2005), which usually represents the main pathway for the formation of GEM available for volatilisation (Cao et al., 2024; Eckley et al., 2021). Consequently, the increase in incident radiation results in a rapid increase in GEM fluxes, as observed in several studies (Floreani et al., 2023b; García-Sánchez et al., 2006; Li et al., 2018; Sizmur et al., 2017). In this study, excluding a few measurements conducted in shaded conditions ($n = 20$), GEM fluxes showed a weak but statistically significant correlation with mean UV radiation measured during sampling ($\tau = 0.37$, $p < 0.0001$, $n = 143$; Fig. S4a). Moreover, considering temporal variation, higher peak GEM fluxes generally coincided with maximum UV intensity between 11:00 and 16:00 (Fig. 2).

Only 18 flux measurements (~11% of the total) were taken with UV incident radiation below 15 W m^{-2}, < 70% of the daily maximum. These measurements were mostly taken in the early morning (approximately before 9:00) at the beginning of sampling activity and in the late afternoon (after 18:00) only at the DV3 macro-area. Despite low incident UV radiation, relatively high GEM fluxes were still measured during these periods (Fig. 2), reaching values up to 63.1 (DV2-10), 74.4 (DV6-1), and 224 ng m^{-2} h^{-1} (DV1-1) in the early morning period and to 47.9 ng m^{-2} h^{-1} (DV3-35) in the late afternoon. This evidence confirms a noticeable GEM emission even under these conditions.

In addition to promoting Hg^{2+} photo-reduction, incident solar radiation contributes to soil heating, which in turn can enhance GEM emission to the atmosphere. This results in a synergic effect of radiation and temperature on GEM fluxes (Bahlmann et al., 2006; Eckley et al., 2015). Temperature can affect GEM fluxes from soils both indirectly, providing energy to catalyse both Hg^{2+} desorption from organic and mineral soil surfaces and biotic and abiotic reduction reactions (Pannu et al., 2014; Sigler and Lee, 2006), and directly by favouring the diffusion of GEM through the soil thanks to the expansion of gases in pores

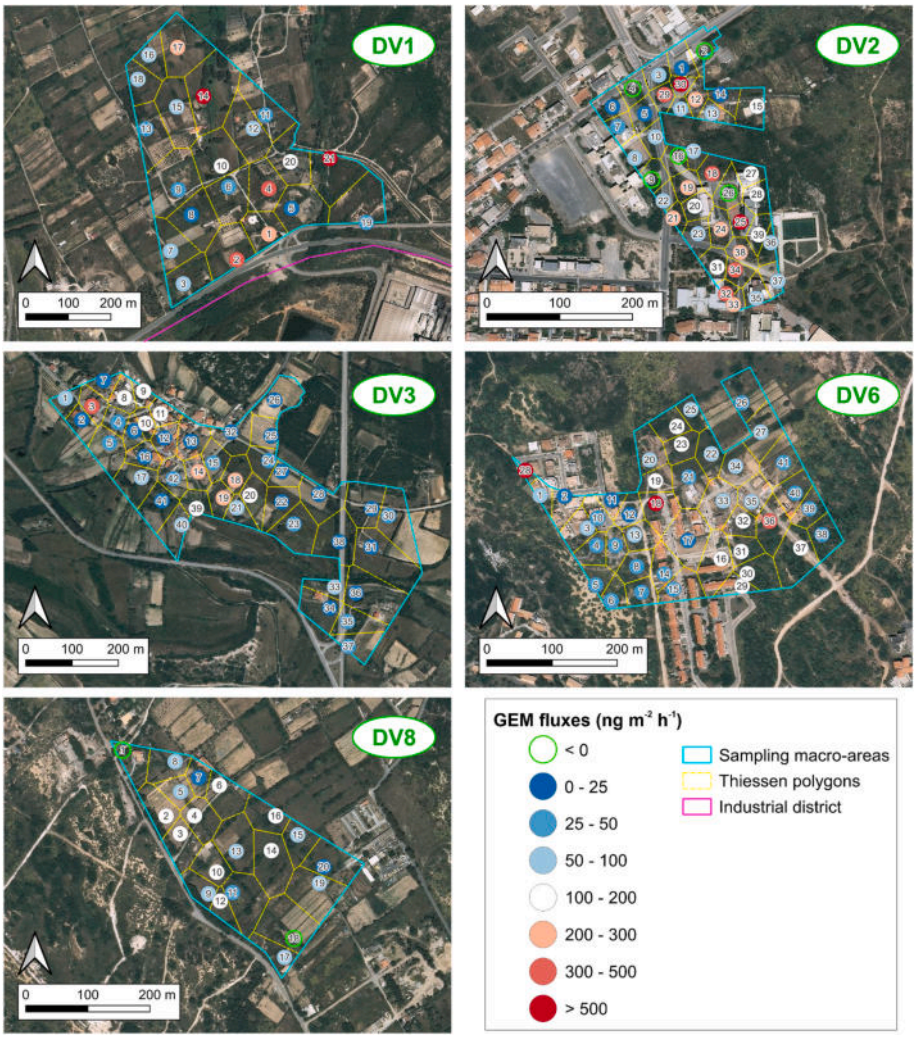

Fig. 5. Spatial distribution of measured GEM fluxes in the five selected macro-areas.

(Schlüter, 2000; Shi et al., 2020). In our case, a weak but statistically significant correlation was observed between air temperature and GEM fluxes ($\tau = 0.24$, $p < 0.0001$, $n = 163$; Fig. S4b) similar to that which has been previously observed in other studies (Edwards and Howard, 2013; Osterwalder et al., 2018; Wallschläger et al., 1999).

The relationship of GEM fluxes with air temperature is weaker than that found with UV radiation, suggesting that the effect of radiation on GEM releases is greater and partially independent compared to that of temperature, in agreement with the evidence found in previous studies (Agnan et al., 2016; Cao et al., 2024; Floreani et al., 2023b; Wang et al., 2005). Due to highly skewed data, a multiple linear regression model was fitted on log-transformed data to assess the relative contribution of the available measured variables (UV radiation, air temperature, CO_2 fluxes) on observed GEM fluxes variability. The obtained model explained 23.1% of variance in GEM fluxes ($R^2 = 0.231$, $F_{3,159} = 18.0$, $p < 0.001$). Assuming that a substantial fraction of the spatial variability of GEM fluxes in Hg-contaminated sites is typically attributed to soil Hg concentrations and soil physical characteristics rather than meteorological variables (Agnan et al., 2016; Rinklebe et al., 2010), this relatively modest proportion of variance explained by the available parameters could be considered as a measure of the influence of only environmental conditions on the observed variability.

Given the significant correlation between UV radiation and air temperature ($\tau = 0.50$, $p < 0.0001$, $n = 163$), dominance analysis was applied to quantify the relative contribution of each variable independently of their intercorrelation. As expected, UV radiation was found to be the dominant predictor, accounting for 54.7% of the variance explained by the model, followed by air temperature (28.7%). However, due to the high collinearity between these two parameters, the independent contribution of temperature could not be reliably estimated from the available data. Despite the low variability in air temperatures, higher GEM fluxes were generally observed in the afternoon compared to the morning at the same level of UV radiation (e.g. at the DV2 and DV6 macro-areas, Fig. 2), coupled with higher temperatures (Sizmur et al., 2017). A temperature-driven increase in GEM fluxes may be linked to processes occurring in deeper soil layers that are not directly influenced by solar radiation, which are particularly relevant in sandy soils (Mazur et al., 2015) like those in our study area. Soil temperature, which can be more indicative of the effect of heating on in-soil processes involved in GEM evasion (Edwards and Howard, 2013), was not measured in this study. However, assuming that CO_2 fluxes can be considered indicative of biotic processes occurring within soil (e.g. respiration), the lack of correlation between GEM and CO_2 fluxes suggests that biotic processes play a limited role in Hg reduction and evasion in our study area. This is further confirmed by the low contribution of CO_2 fluxes to the explained variance of GEM fluxes obtained through dominance analysis (16.5%). The effect of temperature may therefore be more pronounced on abiotic physical processes that regulate GEM exchange, but this hypothesis should be further investigated through additional studies.

Other than meteorological parameters, GEM flux variability can be affected by site-specific conditions related to land-use, particularly in

terms of soil cover and disturbance. To evaluate this aspect, sampling points were divided into 3 different categories according to land-use: i) "Rural": areas characterised by natural vegetation or perennial crops rarely disturbed by agricultural practices; ii) "Arable": farmland subject to periodic ploughing and harvesting; iii) "Urban" within the town of Portoscuso. Moreover, shaded measuring points in rural and urban contexts were considered separately, whereas all measurement in arable areas were conducted under direct sunlight. The distribution of GEM fluxes recorded in these different contexts is represented in Fig. 3b.

The highest GEM fluxes (median = 110 ng m^{-2} h^{-1}) were observed for urban environments, mostly located near the Portovesme industrial complex and thus likely subject to stronger past inputs of Hg through atmospheric depositions. Moreover, the two highest single GEM fluxes were recorded at points included in this category (DV6-28 and DV2-30, 3164 and 2309 ng m^{-2} h^{-1} respectively) and identified as potential outliers (Fig. 3b). Both measurements were taken in areas recently disturbed by nearby construction work and characterised by a lack of vegetation. A similar effect can be caused by soil tilling, as confirmed by relatively high fluxes observed for arable areas in this study. Values calculated for this category were indeed comparable to those found in urban settlements, but significantly higher ($p < 0.01$, Dunn post-hoc test) than those of undisturbed rural soils. Soil physical disturbance can modify the physical structure of the surface layer, enhancing the total area of the soil-air interface and increasing soil porosity and surface roughness. As a result, the diffusion of GEM through the soil-air interface is in turn favoured (Fu et al., 2012). These findings highlight the potential impact of soil management practices on GEM re-emissions at this contaminated site.

Overall, rural environments characterised by Mediterranean scrubland and perennial crops showed lower GEM fluxes (Table S3), likely due to lower Hg supplies compared to urban settlements. However, some single plots in this category showed relatively high GEM fluxes, up to 1032 and 530 ng m^{-2} h^{-1} (DV1-21 and DV1-14, respectively). These points, identified as outliers for the rural environments, were located in the macro-area closest to Portovesme and may therefore have been more susceptible to Hg supplies, mostly DV1-21 which was situated near a road.

Finally, both for rural and urban environments, fluxes measured from shaded plots were lower than those calculated for points under direct sunlight, further confirming the role of solar radiation in promoting the evasion of GEM at the soil-air interface.

3.3. Risk assessment

In the outdoor scenarios, acceptable GEM emission rates (F_{acc}) depend inversely on the size of the emitting area. Therefore, for the same receptors and exposure parameters, the F_{acc} assessed at the scale of the entire macro-area is more precautionary than that calculated for each single polygon. Based on the selected exposure parameters (Table S1), the F_{acc} calculated for the outdoor scenarios in the 5 macro-areas are 3 to 5 orders of magnitude higher than those estimated for the indoor environment (Table 2). For all areas, the F_{acc} computed for the indoor scenario (335 ng m^{-2} h^{-1}) is the same, due to the fact that the modelling estimate in this case is not a function of the size of the emitting area but is influenced by other parameters (i.e. local building types and exposure standards).

The specific GEM emission rates calculated for each macro-area on the basis of field measurements varied between 85.8 and 210 ng m^{-2} h^{-1} (Table 2): these values are 3 or more orders of magnitude lower than the F_{acc} for all the outdoor scenarios and only slightly lower than the F_{acc} estimated for the indoor scenarios. As the purpose of this calculation was to assess the contribution of only GEM re-emitted from the soil surface to potential exposure through inhalation, points showing negative fluxes were considered as 0 ng m^{-2} h^{-1} (no emission) in this stage. Excluding the negative values, fluxes measured for each individual polygon ranged between 3.54 and 3164 ng m^{-2} h^{-1}, consistently lower than the estimated F_{acc} for all the outdoor exposure scenarios. Conversely, only 8 points (4.9% of the total) randomly scattered across the study area showed GEM fluxes higher than the acceptable level for indoor scenarios (Fig. 6). These measurements can indicate localised anomalies related to indoor exposure in more sensitive scenarios (i.e. residential) but are generally not indicative of an actual diffuse unacceptable risk over the whole study area. It is also worth noting that the uncertainty associated with flux-derived exposure estimates should be interpreted within the broader context of human health risk assessment. Even when detailed site-specific data are available (e.g. measured air concentrations), estimated risk levels cannot be directly validated unless real human exposure and health outcomes are assessed, for instance through biomonitoring and epidemiological evidence. Risk assessment therefore inherently relies on conservative assumptions and on dose-response relationships derived from controlled experimental studies and extrapolated to humans.

Within this framework, uncertainties related to environmental modelling choices or field measurements represent only one component of a more complex uncertainty structure. Consequently, the conservative assumptions adopted in this study are consistent with standard risk-based decision frameworks commonly applied to contaminated sites.

Moreover, it must be stressed that as a precautionary approach, exposure in the indoor scenario was estimated considering an exposure time $\geq$ 18 h d^{-1} for several years (Table S1) to compensate for uncertainties related to flux variability and simplified exposure modelling. This may have led to an overestimation of the real risk considering that calculations are based on GEM flux data measured in the worst-case conditions (high radiation and temperature) and that fluxes during nights and colder seasons are expected to be significantly lower than those observed in this study during daytime in late spring (Polyzou et al., 2019; Shi et al., 2020; Wang et al., 2005). A rapid increase in GEM fluxes can be expected only after rain events due to the physical displacement of GEM present in soil gas by the infiltration of water (Briggs and Gustin, 2013). Rainfall leads to a sudden significant increase in GEM fluxes mostly in dry soils, whereas this effect is less evident in soils with initial higher moisture content (Song and Van Heyst, 2005). After precipitation, GEM fluxes are controlled by the upward movement of water vapour, which transports Hg to the soil surface where it is more available for volatilisation. As the soil dries and soil tension increases, GEM fluxes decline as the evaporation rate decreases. Consequently, in soils that dry out quickly, the return of fluxes to the baseline level is very rapid (Gustin and Stamenkovic, 2005). As this process is strongly

Table 2
Specific GEM emission rates (F_{spec}) and acceptable GEM fluxes (F_{acc}) estimated for the five selected macro-areas under different scenarios. For the outdoor environments, out_RES: residential; out_RES-AGR: mixed residential-agricultural; out_RIC: recreational; out_RIC-PAS: pasture.

Area	Surface (m^2)	F_{spec} (ng m^{-2} h^{-1})	F_{acc} (ng m^{-2} h^{-1})				
			indoor	out_RES	out_RES-AGR	out_RIC	out_RIC-PAS
DV1	208,619	$1.89 \cdot 10^2$	$3.35 \cdot 10^2$	$1.45 \cdot 10^5$	$1.86 \cdot 10^5$	$4.92 \cdot 10^5$	$6.92 \cdot 10^6$
DV2	46,387	$2.10 \cdot 10^2$	$3.35 \cdot 10^2$	$3.08 \cdot 10^5$	$3.97 \cdot 10^5$	$1.05 \cdot 10^6$	$1.47 \cdot 10^7$
DV3	126,878	$8.58 \cdot 10^1$	$3.35 \cdot 10^2$	$1.86 \cdot 10^5$	$2.40 \cdot 10^5$	$6.33 \cdot 10^5$	$8.88 \cdot 10^6$
DV6	94,772	$1.04 \cdot 10^2$	$3.35 \cdot 10^2$	$2.15 \cdot 10^5$	$2.78 \cdot 10^5$	$7.33 \cdot 10^5$	$1.03 \cdot 10^7$
DV8	67,366	$9.25 \cdot 10^1$	$3.35 \cdot 10^2$	$2.55 \cdot 10^5$	$3.29 \cdot 10^5$	$8.67 \cdot 10^5$	$1.22 \cdot 10^7$

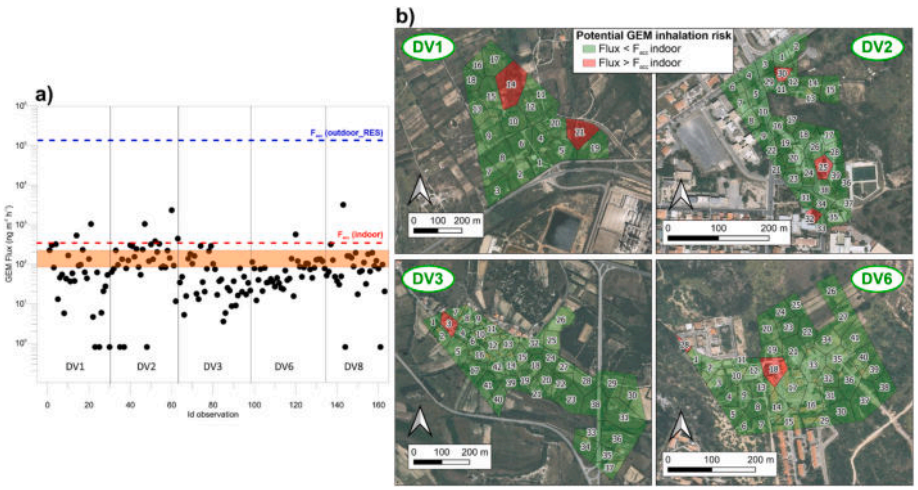

Fig. 6. a) Measured GEM emissions compared with acceptable values for indoor and outdoor scenarios. For the latter case, the lowest threshold flux is shown (residential land use). The orange band represents the range of specific GEM emissions calculated at the scale of entire macro-areas. b) spatial distribution of GEM fluxes higher than acceptable threshold for the indoor scenario. Within the DV8 macro-area (not shown) all GEM fluxes were below F_{acc}. (For interpretation of the references to colour in this figure legend, the reader is referred to the Web version of this article.)

dependent on soil texture (Briggs and Gustin, 2013), it can be assumed that in sandy soils of the studied area, the potential increase of GEM fluxes after precipitation will only occur for a limited time after rainfall.

Overall, these results indicate that GEM re-emissions at the soil-air interface in this area do not pose an immediate health risk for local inhabitants through inhalation of GEM since, according to these simulations, they are not expected to cause the occurrence of potentially harmful atmospheric GEM concentrations.

4. Conclusions

Overall, GEM fluxes measured at the soil-air interface within Portoscuso showed a remarkable spatial variability, with relatively high emissions observed only in some isolated measuring points. Measured values are comparable to those reported for other historically contaminated soils, supporting the evidence that these soils represent a long-term secondary source of GEM to the atmosphere. The observed strong spatial variability of GEM fluxes is related to the complexity of the investigated area, characterised by a wide range of environmental conditions from urban to natural contexts, and only partially to the distance from the contamination source. Despite this, a relationship between GEM fluxes and UV radiation and temperature has been observed, thus confirming the influence of these meteorological parameters on GEM emission.

A preliminary spatial characterisation of GEM fluxes in highly heterogeneous environmental contexts such that of our study area may indeed be helpful to properly select the more representative locations for the evaluation of the mechanisms regulating GEM exchanges in each environmental condition occurring in a contaminated site. Thanks to the brief duration of NSS chamber measurements (~5 min), it is indeed possible to increase the number of sampling locations. As a result, highly localised anomalies of high GEM emissions in the study areas could be identified, which are both worthy of long-term monitoring and potentially more representative of the site-specific combined effect of the various factors influencing GEM fluxes.

Although this approach remains unsuitable for ecosystem-scale studies given its low temporal representativeness, these results indicate that it may be useful for preliminary large-scale screening of GEM fluxes in contaminated areas aimed at identifying possibly more critical areas or land-use practices (e.g. recently ploughed fields in our case) in terms of potential health risk. This evidence can be helpful in supporting a more targeted selection of points worthy of prolonged monitoring and of the most appropriate contamination management practices or any necessary remediation measures.

Excluding the above-mentioned anomalies, GEM re-emissions from soils within our study area are lower than the estimated threshold for human health risk, calculated as the GEM flux capable of generating potentially harmful air concentrations according to the model estimation. Consequently, adverse effects on human health related only to inhalation exposure to GEM re-emitted from soils can be excluded. This conclusion is further strengthened by the fact that measurements were conducted under the worst-case scenario corresponding to the conditions promoting maximum GEM emission from soil (i.e. high radiation and temperature). Thus, the obtained values can be considered indicative of the maximum emissions expected in this historically contaminated area. The conclusions of this study should be interpreted within the context of a risk-based stepwise assessment for contaminated sites. The absence of significant health risk refers to the lack of evidence for unacceptable inhalation risk under deliberately conservative assumptions, applied to the most contaminated areas and designed to prevent false-negative outcomes. In this framework, the results provide robust support for sustainable site management decisions.

CRediT authorship contribution statement

Federico Floreani: Writing – review & editing, Writing – original draft, Visualization, Methodology, Investigation, Formal analysis, Data curation. **Antonella Vecchio:** Writing – original draft, Validation, Supervision, Investigation, Formal analysis, Conceptualization, Writing – review & editing. **Maurizio Guerra:** Writing – original draft, Validation, Supervision, Investigation, Formal analysis, Conceptualization, Writing – review & editing. **Elisa Mariani:** Writing – review & editing, Validation, Investigation, Formal analysis. **Gianfranco Mulas:** Resources, Investigation. **Stefano Covelli:** Writing – review & editing, Validation, Resources, Methodology. **Luca Spinelli:** Validation, Resources, Methodology, Investigation, Data curation, Conceptualization, Writing – review & editing. **Giorgio Virgili:** Writing – review & editing, Validation, Methodology, Investigation, Data curation, Conceptualization.

Declaration of competing interest

The authors declare that they have no known competing financial interests or personal relationships that could have appeared to influence the work reported in this paper.

Acknowledgements

The authors wish to thank the Municipality of Portoscuso for supporting the project and for the assistance provided during fieldwork. Karry Close is warmly acknowledged for proofreading the manuscript. We are also very grateful to the Associate Editor and to the two anonymous reviewers for their thorough reviews and useful suggestions which improved the earlier version of the manuscript.

Appendix A. Supplementary data

Supplementary data to this article can be found online at https://doi.org/10.1016/j.envpol.2026.128400.

Data availability

Data will be made available on request.

References

Acquavita, A., Biasiol, S., Lizzi, D., Mattassi, G., Pasquon, M., Skert, N., Marchiol, L., 2017. Gaseous elemental mercury level and distribution in a heavily contaminated site: the Ex-chlor alkali plant in torviscosa (northern Italy). Water. Air. Soil Pollut. 228. https://doi.org/10.1007/s11270-016-3234-z.

Agnan, Y., Le Dantec, T., Moore, C.W., Edwards, G.C., Obrist, D., 2016. New constraints on terrestrial surface-atmosphere fluxes of gaseous elemental mercury using a global database. Environ. Sci. Technol. 50, 507–524. https://doi.org/10.1021/acs.est.5b04013.

APAT, 2008. Piano Di Caratterizzazione Aree Esterne Al Polo Industriale Di Portovesme, Comune Di Portoscuso (CI). PdC/EME 14/2008 (in Italian).

Ariya, P.A., Amyot, M., Dastoor, A., Deeds, D., Feinberg, A., Kos, G., Poulain, A., Ryjkov, A., Semeniuk, K., Subir, M., Toyota, K., 2015. Mercury physicochemical and biogeochemical transformation in the atmosphere and at atmospheric interfaces: a review and future directions. Chem. Rev. 115, 3760–3802. https://doi.org/10.1021/cr500667e.

ARPAS, 2020. Climatologia Della Sardegna per Il Trentennio 1981-2010. Relazione Tecnica (in italian).

Aru, A., Baldaccini, P., Vacca, A., Delogu, G., Dessena, M.A., Madrau, S., Melis, R.T., Vacca, S., 1991. Nota Illustrativa Alla Carta Dei Suoli Della Sardegna.

ASTM, 2001. ASTM D5314-92 (2001): Standard Guide for Soil Gas Monitoring in the Vadose Zone. ASTM International, West Conshohocken, PA.

Bacchetta, G., Bagella, S., Biondi, E., Casti, M., Farris, E., Filigheddu, R.S., Iiriti, G., Pontecorvo, C., 2009. Carta Delle Serie Di Vegetazione Della Sardegna. Scala 1: 350.000. Fitosociologia.

Bagnato, E., Barra, M., Cardellini, C., Chiodini, G., Parello, F., Sprovieri, M., 2014. First combined flux chamber survey of mercury and CO2 emissions from soil diffuse degassing at solfatara of Pozzuoli crater, Campi Flegrei (Italy): mapping and quantification of gas release. J. Volcanol. Geoth. Res. 289, 26–40. https://doi.org/10.1016/j.jvolgeores.2014.10.017.

Bain, W.G., Hutyra, L., Patterson, D.C., Bright, A.V., Daube, B.C., Munger, J.W., Wofsy, S. C., 2005. Wind-induced errors in the measurement of soil respiration using closed dynamic chambers. Agric. For. Meteorol. 131, 225–232, 1.1016/j.agrformet.2005.06.004.

Bahlmann, E., Ebinghaus, R., Ruck, W., 2006. Development and application of a laboratory flux measurement system (LFMS) for the investigation of the kinetics of mercury emissions from soils. J. Environ. Manag. 81, 114–125. https://doi.org/10.1016/j.jenvman.2005.09.022.

Bavec, Š., Gosar, M., Biester, H., Grčman, H., 2015. Geochemical investigation of mercury and other elements in urban soil of Idrija (Slovenia). J. Geochem. Explor. 154, 213–223. https://doi.org/10.1016/j.gexplo.2014.10.011.

Beckers, F., Rinklebe, J., 2017. Cycling of mercury in the environment: sources, fate, and human health implications: a review. Crit. Rev. Environ. Sci. Technol. 47, 693–794. https://doi.org/10.1080/10643389.2017.1326277.

Biester, H., Gosar, M., Covelli, S., 2000. Mercury speciation in sediments affected by dumped mining residues in the drainage area of the Idrija mercury mine, Slovenia. Environ. Sci. Technol. 34, 3330–3336. https://doi.org/10.1021/es991334v.

Briggs, C., Gustin, M.S., 2013. Building upon the conceptual model for soil mercury flux: evidence of a link between moisture evaporation and Hg evasion. Water. Air. Soil Pollut. 224, 1744. https://doi.org/10.1007/s11270-013-1744-5.

Bustos Navarrete, C., Coutinho Soares, F., 2025. Dominanceanalysis: dominance analysis. R package version 2.1.1. https://CRAN.R-project.org/package=dominanceanalysis.

Cabassi, J., Venturi, S., Di Bennardo, F., Nisi, B., Tassi, F., Magi, F., Ricci, A., Picchi, G., Vaselli, O., 2021. Flux measurements of gaseous elemental mercury (GEM) from the geothermal area of "Le Biancane" natural park (Monterotondo Marittimo, Grosseto, Italy): Biogeochemical processes controlling GEM emission. J. Geochem. Explor. 228, 106824. https://doi.org/10.1016/j.gexplo.2021.106824.

Canu, S., Rosati, L., Fiori, M., Motroni, A., Filigheddu, R., Farris, E., 2015. Bioclimate map of Sardinia (Italy). J. Maps 11, 711–718. https://doi.org/10.1080/17445647.2014.988187.

Cao, Q., Hu, H., Yuan, W., Huang, J.-H., Fu, X., Feng, X., 2024. Isotope-based characterization of soil elemental mercury emissions from historical mercury mining areas: driving pathways and relative contributions. Environ. Sci. Technol. 58, 16824–16832. https://doi.org/10.1021/acs.est.4c05220.

Cardellini, C., Chiodini, G., Frondini, F., Granieri, D., Lewicki, J., Peruzzi, L., 2003. Accumulation chamber measurements of methane fluxes: application to volcanic-geothermal areas and landfills. Appl. Geochem. 18, 45–54. https://doi.org/10.1016/S0883-2927(02)00091-4.

Carpi, A., Fostier, A.H., Orta, O.R., dos Santos, J.C., Gittings, M., 2014. Gaseous mercury emissions from soil following forest loss and land use changes: field experiments in the United States and Brazil. Atmos. Environ. 96, 423–429. https://doi.org/10.1016/j.atmosenv.2014.08.004.

Carpi, A., Frei, A., Cocris, D., McCloskey, R., Contreras, E., Ferguson, K., 2007. Analytical artifacts produced by a polycarbonate chamber compared to a Teflon chamber for measuring surface mercury fluxes. Anal. Bioanal. Chem. 388, 361–365. https://doi.org/10.1007/s00216-006-1111-0.

Chiodini, G., Cioni, R., Guidi, M., Raco, B., Marini, L., 1998. Soil CO2 flux measurements in volcanic and geothermal areas. Appl. Geochem. 13, 543–552. https://doi.org/10.1016/S0883-2927(97)00076-0.

Conen, F., Smith, K.A., 1998. A re-examination of closed flux chamber methods for the measurement of trace gas emissions from soils to the atmosphere. Eur. J. Soil Sci. 49, 701–707. https://doi.org/10.1046/j.1365-2389.1998.4940701.x.

Di Francesco, F., Ferrara, R., Mazzolai, B., 1998. Two ways of using a chamber for mercury flux measurement - a simple mathematical approach. Sci. Total Environ. 213, 33–41. https://doi.org/10.1016/S0048-9697(98)00068-0.

Dietzen, C., Rosing, M.T., 2023. Quantification of CO2 uptake by enhanced weathering of silicate minerals applied to acidic soils. Int. J. Greenh. Gas Control 125, 103872. https://doi.org/10.1016/j.ijggc.2023.103872.

During, A., Rinklebe, J., Böhme, F., Wennrich, R., Stärk, H.-J., Mothes, S., Du Laing, G., Schulz, E., Neue, H.-U., 2009. Mercury volatilization from three floodplain soils at the central Elbe River, Germany. Soil Sediment Contam. An Int. J. 18, 429–444. https://doi.org/10.1080/15320380902962395.

Eckley, C.S., Blanchard, P., McLennan, D., Mintz, R., Sekela, M., 2015. Soil-air mercury flux near a large industrial emission source before and after closure (flin flon, Manitoba, Canada). Environ. Sci. Technol. 49, 9750–9757. https://doi.org/10.1021/acs.est.5b01995.

Eckley, C.S., Eagles-Smith, C., Tate, M.T., Krabbenhoft, D.P., 2021. Surface-air mercury fluxes and a watershed mass balance in forested and harvested catchments. Environ. Pollut. 277, 116869. https://doi.org/10.1016/j.envpol.2021.116869.

Eckley, C.S., Gilmour, C.C., Janssen, S., Luxton, T.P., Randall, P.M., Whalin, L., Austin, C., 2020. The assessment and remediation of mercury contaminated sites: a review of current approaches. Sci. Total Environ. 707, 136031. https://doi.org/10.1016/j.scitotenv.2019.136031.

Eckley, C.S., Gustin, M., Lin, C.J., Li, X., Miller, M.B., 2010. The influence of dynamic chamber design and operating parameters on calculated surface-to-air mercury fluxes. Atmos. Environ. 44, 194–203. https://doi.org/10.1016/j.atmosenv.2009.10.013.

Eckley, C.S., Gustin, M., Marsik, F., Miller, M.B., 2011. Measurement of surface mercury fluxes at active industrial gold mines in Nevada (USA). Sci. Total Environ. 409, 514–522. https://doi.org/10.1016/j.scitotenv.2010.10.024.

Edwards, G.C., Howard, D.A., 2013. Air-surface exchange measurements of gaseous elemental mercury over naturally enriched and background terrestrial landscapes in Australia. Atmos. Chem. Phys. 13, 5325–5336. https://doi.org/10.5194/acp-13-5325-2013.

Elío, J., Ortega, M.F., Nisi, B., Mazadiego, L.F., Vaselli, O., Caballero, J., Chacón, E., 2016. A multi-statistical approach for estimating the total output of CO2 from diffuse soil degassing by the accumulation chamber method. Int. J. Greenh. Gas Control 47, 351–363. https://doi.org/10.1016/j.ijggc.2016.02.012.

Enrico, M., Le Roux, G., Heimbürger, L.E., Van Beek, P., Souhaut, M., Chmeleff, J., Sonke, J.E., 2017. Holocene atmospheric mercury levels reconstructed from peat bog mercury stable isotopes. Environ. Sci. Technol. 51, 5899–5906. https://doi.org/10.1021/acs.est.6b05804.

Esbrí, J.M., Cacovean, H., Higueras, P., 2018. Usage proposal of a common urban decorative tree (Salix alba L.) to monitor the dispersion of gaseous mercury: a case study from Turda (Romania). Chemosphere 193, 74–81. https://doi.org/10.1016/j.chemosphere.2017.11.007.

Esbrí, J.M., Higueras, P.L., Martínez-Coronado, A., Naharro, R., 2020. 4D dispersion of total gaseous mercury derived from a mining source: identification of criteria to assess risks related to high concentrations of atmospheric mercury. Atmos. Chem. Phys. 20, 12995–13010. https://doi.org/10.5194/acp-20-12995-2020.

Fantozzi, L., Ferrara, R., Dini, F., Tamburello, L., Pirrone, N., Sprovieri, F., 2013. Study on the reduction of atmospheric mercury emissions from mine waste enriched soils through native grass cover in the mt. Amiata region of Italy. Environ. Res. 125, 69–74. https://doi.org/10.1016/j.envres.2013.02.004.

FAO and IIASA, 2008. Harmonized world soil database version 2.0. Rome and Laxenburg. https://doi.org/10.4060/cc3823en.

Fitzgerald, W.F., Clarkson, T.W., 1991. Mercury and monomethylmercury: present and future concerns. Environ. Health Perspect. 96, 159–166. https://doi.org/10.1289/ehp.9196159.

Floreani, F., Acquavita, A., Barago, N., Klun, K., Faganeli, J., Covelli, S., 2022. Gaseous mercury exchange from water – air interface in differently impacted freshwater environments. Int. J. Environ. Res. Publ. Health 19, 8149. https://doi.org/10.3390/ijerph19138149.

Floreani, F., Pavoni, E., Gosar, M., Covelli, S., 2023a. Evasion of gaseous elemental mercury from forest and urban soils contaminated by historical and modern ore

roasting processes (Idrija, Slovenia). Atmosphere 14, 1036. https://doi.org/10.3390/atmos14061036.
Floreani, F., Zappella, V., Faganeli, J., Covelli, S., 2023b. Gaseous mercury evasion from bare and grass-covered soils contaminated by mining and ore roasting (Isonzo River alluvial plain, Northeastern Italy). Environ. Pollut. 318, 120921. https://doi.org/10.1016/j.envpol.2022.120921.
Fritsche, J., Obrist, D., Alewell, C., 2008. Evidence of microbial control of Hg0 emissions from uncontaminated terrestrial soils. J. Plant Nutr. Soil Sci. 171, 200–209. https://doi.org/10.1002/jpln.200625211.
Fu, X., Feng, X., Zhang, H., Yu, B., Chen, L., 2012. Mercury emissions from natural surfaces highly impacted by human activities in Guangzhou province, South China. Atmos. Environ. 54, 185–193. https://doi.org/10.1016/j.atmosenv.2012.02.008.
Gallego, E., Perales, J.F., Roca, F.J., Guardino, X., 2014. Surface emission determination of volatile organic compounds (VOC) from a closed industrial waste landfill using a self-designed static flux chamber. Sci. Total Environ. 470–471, 587–599. https://doi.org/10.1016/j.scitotenv.2013.09.105.
García-Sánchez, A., Contreras, F., Adams, M., Santos, F., 2006. Atmospheric mercury emissions from polluted gold mining areas (Venezuela). Environ. Geochem. Health 28, 529–540. https://doi.org/10.1007/s10653-006-9049-x.
Gillis, A., Miller, D.R., 2000. Some potential errors in the measurement of mercury gas exchange at the soil surface using a dynamic flux chamber. Sci. Total Environ. 260, 181–189. https://doi.org/10.1016/S0048-9697(00)00562-3.
Grangeon, S., Guédron, S., Asta, J., Sarret, G., Charlet, L., 2012. Lichen and soil as indicators of an atmospheric mercury contamination in the vicinity of a chlor-alkali plant (Grenoble, France). Ecol. Indic. 13, 178–183. https://doi.org/10.1016/j.ecolind.2011.05.024.
Gustin, M.S., Biester, H., Kim, C.S., 2002. Investigation of the light-enhanced emission of mercury from naturally enriched substrates. Atmos. Environ. 36, 3241–3254. https://doi.org/10.1016/S1352-2310(02)00329-1.
Gustin, M.S., Stamenkovic, J., 2005. Effect of watering and soil moisture on mercury emissions from soils. Biogeochemistry 76, 215–232. https://doi.org/10.1007/s10533-005-4566-8.
Heinemeyer, A., McNamara, N.P., 2011. Comparing the closed static versus the closed dynamic chamber flux methodology: implications for soil respiration studies. Plant Soil 346, 145–151. https://doi.org/10.1007/s11104-011-0804-0.
Huremović, J., Horvat, M., Kotnik, J., Kocman, D., Žižek, S., Ribeiro Guevara, S., Muhić-Šarac, T., Memić, M., 2017. Characterization of mercury contamination surrounding a chloralkali production facility in Tuzla, Bosnia and Herzegovina. Anal. Lett. 50, 1049–1064. https://doi.org/10.1080/00032719.2016.1205595.
Hutchinson, G.L., Livingston, G.P., 2001. Vents and seals in non-steady-state chambers used for measuring gas exchange between soil and the atmosphere. Eur. J. Soil Sci. 52, 675–682. https://doi.org/10.1046/j.1365-2389.2001.00415.x.
Jiskra, M., Wiederhold, J.G., Skyllberg, U., Kronberg, R.M., Hajdas, I., Kretzschmar, R., 2015. Mercury deposition and Re-emission pathways in boreal forest soils investigated with Hg isotope signatures. Environ. Sci. Technol. 49, 7188–7196. https://doi.org/10.1021/acs.est.5b00742.
Johnson, P.C., Ettinger, R.A., 1991. Heuristic model for predicting the intrusion rate of contaminant vapors into buildings. Environ. Sci. Technol. 25, 1445–1452. https://doi.org/10.1021/es00020a013.
Kocman, D., Horvat, M., 2010. A laboratory based experimental study of mercury emission from contaminated soils in the River Idrijca catchment. Atmos. Chem. Phys. 10, 1417–1426. https://doi.org/10.5194/acp-10-1417-2010.
Kocman, D., Horvat, M., Pirrone, N., Cinnirella, S., 2013. Contribution of contaminated sites to the global mercury budget. Environ. Res. 125, 160–170. https://doi.org/10.1016/j.envres.2012.12.011.
Kondo, M., Korre, A., Komai, T., Watanabe, N., 2024. Multi-layered physical factors govern mercury release from soil: implications for predicting the environmental fate of mercury. J. Environ. Manag. 352, 120024. https://doi.org/10.1016/j.jenvman.2024.120024.
Kuzyakov, Y., 2006. Sources of CO2 efflux from soil and review of partitioning methods. Soil Biol. Biochem. 38, 425–448. https://doi.org/10.1016/j.soilbio.2005.08.020.
Kyllönen, K., Hakola, H., Hellén, H., Korhonen, M., Verta, M., 2012. Atmospheric mercury fluxes in a southern boreal forest and wetland. Water. Air. Soil Pollut. 223, 1171–1182. https://doi.org/10.1007/s11270-011-0935-1.
Li, C., Liang, H., Liang, M., Chen, Y., Zhou, Y., 2018. Mercury emissions flux from various land uses in old mining area, Inner Mongolia, China. J. Geochem. Explor. 192, 132–141. https://doi.org/10.1016/j.gexplo.2018.06.011.
Liu, F., Cheng, H., Yang, K., Zhao, C., Liu, Y., Peng, M., Li, K., 2014. Characteristics and influencing factors of mercury exchange flux between soil and air in Guangzhou City. J. Geochem. Explor. 139, 115–121. https://doi.org/10.1016/j.gexplo.2013.09.005.
Livingston, G.P., Hutchinson, G.L., 1995. Enclosure-based measurement of trace gas exchange: applications and sources of error. In: Matson, P.A., Harriss, R.C. (Eds.), Methods in Ecology. Biogenic Trace Gases: Measuring Emissions from Soil and Water. Blackwell Science Oxford, Malden, MA, pp. 14–51.
Llanos, W., Kocman, D., Higueras, P., Horvat, M., 2011. Mercury emission and dispersion models from soils contaminated by cinnabar mining and metallurgy. J. Environ. Monit. 13, 3460–3468. https://doi.org/10.1039/c1em10694e.
Maier, M., Weber, T.K.D., Fiedler, J., Fuß, R., Glatzel, S., Huth, V., Jordan, S., Jurasinski, G., Kutzbach, L., Schäfer, K., Weymann, D., Hagemann, U., 2022. Introduction of a guideline for measurements of greenhouse gas fluxes from soils using non-steady-state chambers. J. Plant Nutr. Soil Sci. 185, 447–461. https://doi.org/10.1002/jpln.202200199.
Mao, H., Cheng, I., Zhang, L., 2016. Current understanding of the driving mechanisms for spatiotemporal variations of atmospheric speciated mercury: a review. Atmos. Chem. Phys. 16, 12897–12924. https://doi.org/10.5194/acp-16-12897-2016.
Mazur, M.E.E., Eckley, C.S., Mitchell, C.P.J., 2015. Susceptibility of soil bound mercury to gaseous emission as a function of source depth: an enriched isotope tracer investigation. Environ. Sci. Technol. 49, 9143–9149. https://doi.org/10.1021/acs.est.5b01747.
Moore, C., Carpi, A., 2005. Mechanisms of the emission of mercury from soil: role of UV radiation. J. Geophys. Res. Atmos. 110, D24302. https://doi.org/10.1029/2004JD005567.
Nacht, D.M., Gustin, M.S., Engle, M.A., Zehner, R.E., Giglini, A.D., 2004. Atmospheric mercury emissions and speciation at the sulphur bank mercury mine superfund site, Northern California. Environ. Sci. Technol. 38, 1977–1983. https://doi.org/10.1021/es0304244.
Oertel, C., Matschullat, J., Zurba, K., Zimmermann, F., Erasmi, S., 2016. Greenhouse gas emissions from soils—A review. Chem. Erde 76, 327–352. https://doi.org/10.1016/j.chemer.2016.04.002.
Osterwalder, S., Huang, J.H., Shetaya, W.H., Agnan, Y., Frossard, A., Frey, B., Alewell, C., Kretzschmar, R., Biester, H., Obrist, D., 2019. Mercury emission from industrially contaminated soils in relation to chemical, microbial, and meteorological factors. Environ. Pollut. 250, 944–952. https://doi.org/10.1016/j.envpol.2019.03.093.
Osterwalder, S., Sommar, J., Åkerblom, S., Jocher, G., Fritsche, J., Nilsson, M.B., Bishop, K., Alewell, C., 2018. Comparative study of elemental mercury flux measurement techniques over a Fennoscandian boreal peatland. Atmos. Environ. 172, 16–25. https://doi.org/10.1016/j.atmosenv.2017.10.025.
Pannu, R., Siciliano, S.D., O'Driscoll, N.J., 2014. Quantifying the effects of soil temperature, moisture and sterilization on elemental mercury formation in boreal soils. Environ. Pollut. 193, 138–146. https://doi.org/10.1016/j.envpol.2014.06.023.
Petranich, E., Predonzani, S., Acquavita, A., Mashyanov, N., Covelli, S., 2022. Rapid thermoscanning technique for direct analysis of mercury species in contaminated sediments : from pure compounds to real sample application. Appl. Geochem. 143, 105393. https://doi.org/10.1016/j.apgeochem.2022.105393.
Polyzou, C., Loupa, G., Trepekli, A., Rapsomanikis, S., 2019. Fluxes of gaseous elemental mercury on a mediterranean coastal grassland. Atmosphere 10, 485. https://doi.org/10.3390/atmos10090485.
Pumpanen, J., Kolari, P., Ilvesniemi, H., Minkkinen, K., Vesala, T., Niinistö, S., Lohila, A., Larmola, T., Morero, M., Pihlatie, M., Janssens, I., Yuste, J.C., Grünzweig, J.M., Reth, S., Subke, J.A., Savage, K., Kutsch, W., Østreng, G., Ziegler, W., Anthoni, P., Lindroth, A., Hari, P., 2004. Comparison of different chamber techniques for measuring soil CO 2 efflux. Agric. For. Meteorol. 123, 159–176. https://doi.org/10.1016/j.agrformet.2003.12.001.
Raich, J.W., Schlesinger, W.H., 1992. The global carbon dioxide flux in soil respiration and its relationship to vegetation and climate. Tellus B 44, 81–99. https://doi.org/10.1034/j.1600-0889.1992.t01-1-00001.x.
R Core Team, 2025. _R: a Language and Environment for Statistical Computing. R Foundation for Statistical Computing, Vienna, Austria. https://www.R-project.org/.
Rinklebe, J., During, A., Overesch, M., Du Laing, G., Wennrich, R., Stärk, H.J., Mothes, S., 2010. Dynamics of mercury fluxes and their controlling factors in large Hg-polluted floodplain areas. Environ. Pollut. 158, 308–318. https://doi.org/10.1016/j.envpol.2009.07.001.
Rinklebe, J., During, A., Overesch, M., Wennrich, R., Stärk, H.J., Mothes, S., Neue, H.U., 2009. Optimization of a simple field method to determine mercury volatilization from soils-Examples of 13 sites in floodplain ecosystems at the Elbe River (Germany). Ecol. Eng. 35, 319–328. https://doi.org/10.1016/j.ecoleng.2008.04.019.
Schintu, M., Cogoni, A., Durante, L., Cantaluppi, C., Contu, A., 2005. Moss (Bryum radiculosum) as a bioindicator of trace metal deposition around an industrialised area in Sardinia (Italy). Chemosphere 60, 610–618. https://doi.org/10.1016/j.chemosphere.2005.01.050.
Schintu, M., Degetto, S., 1999. Sedimentary records of heavy metals in the industrial harbour of Portovesme, Sardinia (Italy). Sci. Total Environ. 241, 129–141. https://doi.org/10.1016/S0048-9697(99)00336-8.
Schlüter, K., 2000. Review: evaporation of mercury from soils. An integration and synthesis of current knowledge. Environ. Geol. 39, 249–271. https://doi.org/10.1007/s002540050005.
Schroder, I.F., Zhang, H., Zhang, C., Feitz, A.J., 2016. The role of soil flux and soil gas monitoring in the characterisation of a CO2 surface leak: a case study in Qinghai, China. Int. J. Greenh. Gas Control 54, 84–95. https://doi.org/10.1016/j.ijggc.2016.07.030.
Selin, H., Keane, S.E., Wang, S., Selin, N.E., Davis, K., Bally, D., 2018. Linking science and policy to support the implementation of the minamata convention on mercury. Ambio 47, 198–215. https://doi.org/10.1007/s13280-017-1003-x.
Selin, N.E., 2009. Global biogeochemical cycling of mercury: a review. Annu. Rev. Environ. Resour. 34, 43–63. https://doi.org/10.1146/annurev.environ.051308.084314.
Shi, T., Gong, Y., Ma, J., Wu, H., Yang, S., Ju, T., Qu, Y., Liu, L., 2020. Soil-air exchange of mercury from agricultural fields in Zhejiang, East China: seasonal variations, influence factors, and models of fluxes. Chemosphere 249, 126063. https://doi.org/10.1016/j.chemosphere.2020.126063.
Sholupov, S., Pogarev, S., Ryzhov, V., 2004. Zeeman Atomic Absorption Spectrometer RA-915 + for Direct Determination of Mercury in Air and Complex Matrix Samples, vol. 85, pp. 473–485. https://doi.org/10.1016/j.fuproc.2003.11.003.
Sigler, J.M., Lee, X., 2006. Gaseous mercury in background forest soil in the northeastern United States. J. Geophys. Res. Biogeosci. 111, G02007. https://doi.org/10.1029/2005JG000106.
Sizmur, T., McArthur, G., Risk, D., Tordon, R., O'Driscoll, N.J., 2017. Gaseous mercury flux from salt marshes is mediated by solar radiation and temperature. Atmos. Environ. 153, 117–125. https://doi.org/10.1016/j.atmosenv.2017.01.024.

SNPA, 2018. In: Procedura Operativa per la Valutazione E L'Utilizzo Dei Dati Derivanti Da Misure Di Gas Interstiziali Nell'Analisi Di Rischio Dei Siti Contaminati (In Italian). Seduta Del 03.10.18. Doc. 41/18. Linee Guida SNPA 17-2018. Rome.

Sommar, J., Osterwalder, S., Zhu, W., 2020. Recent advances in understanding and measurement of Hg in the environment: surface-atmosphere exchange of gaseous elemental mercury (Hg0). Sci. Total Environ. 721, 137648. https://doi.org/10.1016/j.scitotenv.2020.137648.

Song, X., Van Heyst, B., 2005. Volatilization of mercury from soils in response to simulated precipitation. Atmos. Environ. 39, 7494–7505. https://doi.org/10.1016/j.atmosenv.2005.07.064.

Streets, D.G., Horowitz, H.M., Lu, Z., Levin, L., Thackray, C.P., Sunderland, E.M., 2019. Five hundred years of anthropogenic mercury: spatial and temporal release profiles. Environ. Res. Lett. 14, 084004. https://doi.org/10.1088/1748-9326/ab281f.

Sun, R., Hintelmann, H., Wiklund, J.A., Evans, M.S., Muir, D., Kirk, J.L., 2022. Mercury isotope variations in Lake sediment cores in response to direct mercury emissions from non-ferrous metal smelters and legacy mercury remobilization. Environ. Sci. Technol. 56, 8266–8277. https://doi.org/10.1021/acs.est.2c02692.

Sun, Y., Guo, Z., Du, J., Zhao, W., 2020. Diffuse emission and transport of gaseous elemental mercury (GEM) in the Mapamyum geothermal system, Western Tibet (China). J. Volcanol. Geoth. Res. 397, 106825. https://doi.org/10.1016/j.jvolgeores.2020.106825.

Sun, Y., Li, P., Zhang, Y., Zhao, X., Li, Y., Guo, Z., Zhao, W., Xie, X., 2025. Gaseous elemental mercury emissions in the Yangbajing geothermal field, Tibetan Plateau. Appl. Geochem. 193, 106540. https://doi.org/10.1016/j.apgeochem.2025.106540.

Tassi, F., Cabassi, J., Calabrese, S., Nisi, B., Venturi, S., Capecchiacci, F., Giannini, L., Vaselli, O., 2016. Diffuse soil gas emissions of gaseous elemental mercury (GEM) from hydrothermal-volcanic systems: an innovative approach by using the static closed-chamber method. Appl. Geochem. 66, 234–241. https://doi.org/10.1016/j.apgeochem.2016.01.002.

UN Environment, 2019. Global Mercury Assessment 2018. UN Environment Programme. Chemicals and Health Branch, Geneva, Switzerland.

US EPA, 1996. Soil screening guidance : technical background document. EPA/540/R-95/128. Off. Emerg. Remedial Response U.S. Environ. Prot. Agency Washington, DC 20460, 1–49.

Vecchio, A., Guerra, M., Mulas, G., 2015. Risk assessment of the large polluted area in the municipality of Portoscuso, Italy. In: Pérez, A.P., Sánchez, S.P., Van Liedekerke, M. (Eds.), Remediated Sites and Brownfields. Success Stories in Europe. EUR 27530 EN. European Union, pp. 168–175. https://doi.org/10.2788/406096.

Vecchio, A., Guerra, M., Mulas, G., 2012. Manganese and sulphate background in groundwater at Portoscuso (Sardinia): a tool for water management in a large contaminated area. In: Quercia, F.F., Vidojevic, D. (Eds.), Clean Soil and Safe Water. Springer, Netherlands, Dordrecht, pp. 77–90. https://doi.org/10.1007/978-94-007-2240-8.

Wagai, R., Brye, K.R., Gower, S.T., Norman, J.M., Bundy, L.G., 1998. Land use and environmental factors influencing soil surface CO2 flux and microbial biomass in natural and managed ecosystems in southern Wisconsin. Soil Biol. Biochem. 30, 1501–1509. https://doi.org/10.1016/S0038-0717(98)00041-8.

Wallschläger, D., Turner, R.R., London, J., Ebinghaus, R., Kock, H.H., Sommar, J., Xiao, Z., 1999. Factors affecting the measurement of mercury emissions from soils with flux chambers. J. Geophys. Res. Atmos. 104, 21859–21871. https://doi.org/10.1029/1999JD900314.

Wang, S., Feng, X., Qiu, G., Wei, Z., Xiao, T., 2005. Mercury emission to atmosphere from Lanmuchang Hg-Tl mining area, Southwestern Guizhou, China. Atmos. Environ. 39, 7459–7473. https://doi.org/10.1016/j.atmosenv.2005.06.062.

Wang, D., He, L., Shi, X., Wei, S., Feng, X., 2006. Release flux of mercury from different environmental surfaces in Chongqing, China. Chemosphere 64, 1845–1854. https://doi.org/10.1016/j.chemosphere.2006.01.054.

Weissert, L.F., Salmond, J.A., Schwendenmann, L., 2016. Variability of soil organic carbon stocks and soil CO2 efflux across urban land use and soil cover types. Geoderma 271, 80–90. https://doi.org/10.1016/j.geoderma.2016.02.014.

Wickham, H., 2016. ggplot2: Elegant Graphics for Data Analysis, second ed. Springer-Verlag, New York.

Xia, K., Skyllberg, U.L., Bleam, W.F., Bloom, P.R., Nater, E.A., Helmke, P.A., 1999. X-ray absorption spectroscopic evidence for the complexation of Hg(II) by reduced sulfur in soil humic substances. Environ. Sci. Technol. 33, 257–261. https://doi.org/10.1021/es980433q.

Xie, J., Li, Y., Zhai, C., Li, C., Lan, Z., 2009. CO2 absorption by alkaline soils and its implication to the global carbon cycle. Environ. Geol. 56, 953–961. https://doi.org/10.1007/s00254-008-1197-0.

Xu, L., Furtaw, M.D., Madsen, R.A., Garcia, R.L., Anderson, D.J., McDermitt, D.K., 2006. On mantaining pressure equilibrium between a soil CO_2 flux chamber and the ambient air. J. Geophys. Res. Atmos. 111, D08S10. https://doi.org/10.1029/2005JD006435.

Zhao, S., Terada, A., Nakamura, K., Nakashima, M., Komai, T., Riya, S., Hosomi, M., Hou, H., 2022. Significance of soil moisture on temperature dependence of Hg emission. J. Environ. Manag. 305, 114308. https://doi.org/10.1016/j.jenvman.2021.114308.

Zhu, W., Li, Z., Li, P., Yu, B., Lin, C.J., Sommar, J., Feng, X., 2018. Re-emission of legacy mercury from soil adjacent to closed point sources of Hg emission. Environ. Pollut. 242, 718–727. https://doi.org/10.1016/j.envpol.2018.07.002.

Zhu, W., Lin, C.J., Wang, X., Sommar, J., Fu, X., Feng, X., 2016. Global observations and modeling of atmosphere-surface exchange of elemental mercury: a critical review. Atmos. Chem. Phys. 16, 4451–4480. https://doi.org/10.5194/acp-16-4451-2016.